Targeting ZDHHC9 potentiates anti-programmed death-ligand 1 immunotherapy of pancreatic cancer by modifying the tumor microenvironment

Lin, Zhiqing; Huang, Keke; Guo, Hui; Jia, Manli; Sun, Qiuqin; Chen, Xuhao; Wu, Jianmin; Yao, Qingqing; Zhang, Peng; Vakal, Sergii; Zou, Zhengzhi; Gao, Haiyao; Ci, Lei; Chen, Jiangfan; Guo, Wei

Targeting ZDHHC9 potentiates anti-programmed death-ligand 1 immunotherapy of pancreatic cancer by modifying the tumor microenvironment

Zhiqing Lin [a,1], Keke Huang [b,1], Hui Guo [a,1], Manli Jia [a], Qiuqin Sun [a], Xuhao Chen [a], Jianmin Wu [c], Qingqing Yao [d], Peng Zhang [e], Sergii Vakal [f], Zhengzhi Zou [g], Haiyao Gao [h], Lei Ci [h], Jiangfan Chen [a,*], Wei Guo [a,*]

[a] The Molecular Neuropharmacology Laboratory and the Eye-Brain Research Center, The State Key Laboratory of Ophthalmology, Optometry and Vision Science, Wenzhou Medical University, Wenzhou, 325000, China
[b] Department of Ophthalmology, The Third People's Hospital of Chengdu, The Affiliated Hospital of Southwest Jiaotong University, Chengdu, 610031, China
[c] Institute of Genomic Medicine, Wenzhou Medical University, Wenzhou, Zhejiang, 325000, China
[d] Institute of Advanced Materials for Nano-Bio Applications, School of Ophthalmology & Optometry and Eye Hospital, Wenzhou Medical University, Wenzhou, Zhejiang, 325000, China
[e] Shenzhen Key Laboratory of E.N.T., Institute of E.N.T. and Longgang E.N.T. hospital, Shenzhen, Guangdong, 518000, China
[f] Structural Bioinformatics Lab, Department of Biochemistry, Åbo Akademi University, Turku, Southwest Finland, 20100, Finland
[g] MOE Key Laboratory of Laser Life Science & Institute of Laser Life Science, College of Biophotonics, South China Normal University, Guangzhou, Guangdong, 510631, China
[h] Shanghai Model Organisms Center, Inc., Shanghai Engineering Research Center for Model Organisms, Shanghai, 200000, China

ARTICLE INFO

ABSTRACT

Immune checkpoint blockade (ICB) therapy targeting the programmed death 1/programmed death-ligand 1 (PD-1/PD-L1) axis has achieved considerable success in treating a wide range of cancers. However, most patients with pancreatic cancer remain resistant to ICB. Moreover, there is a lack of optimal biomarkers for the prediction of response to this therapy. Palmitoylation is mediated by a family of 23 S-acyltransferases, termed zinc finger Asp-His-His-Cys-type palmitoyltransferases (ZDHHC), which precisely control various cancer-related protein functions and represent promising drug targets for cancer therapy. Here, we revealed that tumor cell-intrinsic ZDHHC9 was overexpressed in pancreatic cancer tissues and associated with impaired anti-tumor immunity. In syngeneic pancreatic tumor models, the knockdown of ZDHHC9 expression suppressed tumor progression and prolonged survival time of mice by modifying the immunosuppressive ('cold') to proinflammatory ('hot') tumor microenvironment. Furthermore, ZDHHC9 deficiency sensitized anti-PD-L1 immunotherapy mainly in a CD8$^+$ T cell dependent manner. Lastly, we employed the *ZDHHC9*-siRNA nanoparticle system to efficiently silence ZDHHC9 in pancreatic tumors. Collectively, our findings indicate that ZDHHC9 overexpression in pancreatic tumors is a mechanism involved in the inhibition of host anti-tumor immunity and highlight the importance of inactivating ZDHHC9 as an effective immunotherapeutic strategy and booster for anti-PD-L1 therapy against pancreatic cancer.

1. Introduction

Pancreatic adenocarcinoma (PAAD) is one of the most lethal malignancies accounting for 331,000 cancer-related deaths annually worldwide. In 2021, It was the third leading cause of cancer-related mortality worldwide, and is expected to rank second by 2030 [1,2]. Current chemotherapeutic drugs, namely gemcitabine plus paclitaxel or FOLFIRINOX (folinic acid, fluorouracil, irinotecan, and oxaliplatin), constitute the preferred first-line systemic treatment for patients with advanced (unresectable or recurrent) PAAD [2,3]. Despite partial clinical benefit observed in some patients in response to currently available chemotherapy strategy, the overall response rate remains unsatisfactory [4,5]. Moreover, current standard treatments (i.e., chemotherapy, surgery, and targeted therapies) for patients with pancreatic cancer are rarely linked to long-term remissions, highlighting the unmet need for new therapeutic options [6,7]. Immune checkpoint blockade (ICB) therapy targeting the programmed death 1/programmed death-ligand 1 (PD-1/PD-L1) axis has achieved considerable success in treating a wide range of cancers over the past decade, allowing a subset of patients to achieve long-term survival [8–11]. Pancreatic cancer is one of the most immune-resistant tumor types, a feature that is determined by its unique genomic landscape where key oncogenic drivers shape a highly immune inhibitory tumor microenvironment (TME) at the earliest stages of tumor development [12]. Notably, the efficacy of ICB in the treatment of pancreatic cancer is hampered by the high rate of primary or acquired resistance, indicating that only a small proportion of patients are responsive to this form of immunotherapy [13]. Thus, uncovering the cellular and molecular determinants of resistance to ICB in pancreatic cancer is critical to improving the efficacy of anti-PD-1/L1 therapy. Cancer cells often develop various molecular mechanisms to subvert anti-tumor immunity in favor of tumor growth and progression [14]. The complex interactions between tumor cells and the TME, and particularly the crosstalk between cancer and immune cells, regulate tumor immunity and the response to ICB [15–17]. In addition, genetic and epigenetic alterations during tumor initiation and progression support tumor-cell-intrinsic factors that encourage tumor cell proliferation whilst altering the TME in favor of immune desertification [18–21]. However, the molecular determinants that describe tumor-immune cell interactions and evasion remain poorly defined, thereby hampering the development of novel and effective ICB treatment strategies against pancreatic cancer.

Tumor-intrinsic oncogenic signalling pathways are complex networks that involve alterations in the activity of genes, protein interactions, signalling, and metabolic networks. These networks are closely orchestrated by dynamic post-translational modifications in both normal and cancer cells. Palmitoylation is a reversible enzyme-driven modification that involves the covalent attachment of fatty acids to cysteine residues in substrate proteins [22]. This modification affects both the integral membrane and soluble proteins, including numerous cancer-associated proteins. Palmitoylation is mediated by a family of 23 S-acyltransferases, namely zinc finger Asp-His-His-Cys-type palmitoyltransferases (ZDHHC), which target over 10 % of the proteome and control various protein functions. These functions include protein maturation, trafficking, anchoring, degradation, and signaling [23,24]. Recent studies suggested a strong rationale for targeting specific ZDHHC enzymes as a promising anti-tumor strategy [25]. Proteins of the ZDHHC family are aberrantly increased in diverse tumor tissues; these elevations are correlated with a poor prognosis for glioblastoma and breast carcinoma [26,27]. Furthermore, genetic inactivation of ZDHHC-proteins (e. g., ZDHHC3, ZDHHC5, ZDHHC17, ZDHHC9, and ZDHHC12), has been associated with therapeutic effects in colon cancer, glioblastoma, leukaemia, and ovarian cancer [26,28–32]. Mechanistically, the ZDHHC family affects tumor progression by increasing the palmitoylation levels of certain key oncogenes (e.g., RAS) and enhancing the activity of proteins involved in melanomagenesis (e.g., melanocortin 1 receptor [MC1R]) [33,34]. ZDHHC9 controls tumor development by directly regulating important cancer-related proteins, such as HRAS and NRAS, by enhancing their plasma membrane affinity [35]. This presents an attractive anti-tumor strategy for targeting potentially undruggable proteins (e.g., RAS and other oncoproteins) through this key post-translational modification. Indeed, it has been shown that the genetic knockout of *ZDHHC9* suppresses in situ tumor formation and cancer progression in T-cell acute lymphoblastic leukemia and chronic granulocytic leukemia [31], as well as inhibits the proliferation of glioblastoma and colorectal cancer cells [30,36]. Nevertheless, thus far, there are no studies investigating the effect of ZDHHC9 on pancreatic cancer. Therefore, it is necessary to determine whether ZDHHC9 can serve as an immunotherapeutic target to control pancreatic cancer progression and potentiate ICB treatment.

In this study, we investigated a molecular and cellular mechanism for inhibiting pancreatic tumor progression and improving the survival of transplantable pancreatic tumor models by *ZDHHC9* knockdown (KD). Poorly immunogenic tumor models were used to evaluate the synergistic effect of ZDHHC9 deficiency and PD-L1 monoclonal antibody (mAb) therapy. Furthermore, to improve the translational potential of the ZDHHC9-based treatment strategy, we developed a *ZDHHC9* small-interfering RNA (siRNA) (si*ZDHHC9*) nanoparticle (NP) delivery system to effectively silence ZDHHC9 and delay tumor progression. Collectively, our results showed that ZDHHC9 deficiency improves responses to PD-L1 blockade and overcomes resistance to immunotherapy. These si*ZDHHC9* NPs elicited synergistic anti-tumor immune effects in combination with an anti-PD-L1 mAb. Mechanistically, *ZDHHC9*[KD] suppressed tumor progression by reprogramming the immunosuppressive ('cold') TME to the favourable pro-inflammatory ('hot') TME. This was evidenced by: i) increased infiltration and activation of anti-tumor immune effector cells (e.g., CD8^{+} T cells); ii) decreased infiltration of CD11b^{+}Gr-1^{+} myeloid-derived suppressor cells (MDSCs); and iii) increased expression of pro-inflammatory cytokines and chemokines. Collectively, our findings reveal the immunomodulatory role of the tumor-intrinsic S-palmitoylation regulator, ZDHHC9, in the inhibition of anti-tumor immunity in pancreatic cancer. We further demonstrated that the inhibition or KD of ZDHHC9 reprograms the TME from being inherently immunosuppressive to assume a pro-inflammatory state. The present findings also validated the use of a ZDHHC9-based treatment system for improving the efficacy of anti-PD-L1 therapy in pancreatic cancer, with implications for other forms of ICB.

2. Materials and methods

2.1. Cell culture and transfection

Mouse pancreatic cancer cell line (Pan02) was purchased from the American Type Culture Collection (Manassas, VA, USA). The KPC cancer cell line, derived from (*Kras*[G12D/+]; *Trp53*[R172H/+]; *Pdx1-Cre*) mice, was obtained from the Model Organisms Center, Inc. (Shanghai, China). All cells were cultured in RPMI 1640 medium or Dulbecco's Modified Eagle Medium, supplemented with 10 % Foetal Bovine Serum (FBS; Excellbio) and 1 % penicillin/streptomycin (Beyotime, China) in a CO_2 incubator at 37 ℃ and 5 % CO_2. The *ZDHHC9* short hairpin RNA (shRNA) lentiviral vector (Beijing TSINGKE Biological Technology Co. Ltd., Beijing, China) was used to establish stable transfection cell lines, namely KPC and Pan02. The following 5'–3' sequences were used: sh*ZDHHC*9#1: CAACCAGATTGTGAAACTGAA; sh*ZDHHC*9#2: GGAAGATGAAGAA-GATGAA; sh*ZDHHC*9#3: GGATGATACTAATAAACTA. Mouse tumor cells (30 % confluency) were incubated in medium containing optimal dilutions of lentivirus mixed with polybrene for 48 h. Thereafter, cells were subjected to puromycin selection to obtain stably transfected cells. The retroviral vector PDS406-pL-RFP-*IRES*-BSD (Beijing TSINGKE Biological Technology Co. Ltd., Beijing, China), was constructed by inserting *Nhe*I and *Asc*I fragments of the full-length mouse ZDHHC9 cDNA into the vector. At 72 h after transfection and blasticidin selection, the cells were harvested for immunoblotting analysis. All cell lines were

authenticated and identified by short tandem repeat profiling and mycoplasma testing, respectively.

2.2. In vivo evaluation of ZDHHC9^{KD} in tumor mouse models

All animal work was approved by the Animal Care Committee of Wenzhou Medical University (Wenzhou, China) (approval number: SYXK 22 Zhejiang Province 2015–0009). NOG (NOD/Shi-scid, IL-2 receptor gamma null) mice (The Vital River Laboratory, Beijing, China), aged 6–8 weeks were allowed to acclimate to colony conditions for at least 7 days prior to conducting experiments. For the preparation of the immunocompetent tumor mouse model, stable cells (Pan02, 5×10^6 or 2×10^6; KPC, 3×10^6) in 100 μL of phosphate-buffered saline (PBS) were subcutaneously injected into the right limb flank of C57BL/6 mice belonging to the *ZDHHC9*^{KD} (sh*ZDHHC9*) group; mice in the shControl group received a non-*ZDHHC9*-targetting control shRNA. For the preparation of the immunodeficiency tumor mouse model, ~5×10^6 sh*ZDHHC9* Pan02 cells and shControl cells in 100 μL PBS were subcutaneously implanted into the right flank of NOG mice. The tumors were monitored every 2–3 days, and the volume of the tumor was calculated according to the following formula: $0.523 \times \text{length} \times \text{width}^2$ (length and width represent the major and minor axes, respectively). Mice were sacrificed when the tumor size or ulceration reached 2000 mm^3 and > 25 % of the surface area, respectively. For the evaluation of therapeutic efficacy in vivo, the mice were euthanized, and tumors were harvested and weighed. Pan02 tumors resected from the immunocompetent mouse models were further isolated for flow cytometry (fluorescence-activated cell sorting [FACS]) analysis to evaluate the immune landscape. Furthermore, the levels of secreted cytokines and chemokines were examined in isolated Pan02 tumors.

2.3. Database evaluation of the immunological status of the TME

The association between ZDHHC9 expression and tumor-infiltrating immune cells (TIICs) in pancreatic adenocarcinoma (PAAD) was investigated using the TIMER (https://cistrome.shinyapps.io/timer/) and TISIDB (http://cis.hku.hk/TISIDB/) databases. The correlation between ZDHHC9 and 124 immunomodulators and pan cancer-associated immune cells was explored using the TISIDB database. The four major immunological characteristics of the TME are: the cancer-immunity cycle, the infiltration levels of TIICs, and the expression of immunomodulators and inhibitory immune checkpoints. PAAD patients were stratified according to the expression of *ZDHHC9* in their tumors, whereby *ZDHHC9* transcript levels were defined as high (above the 60th quartile) and low (below the 40th quartile). We obtained fragments per kilobase million (FPKM) information relating to immunomodulators (including immune stimulators, MHC, receptors, and chemokines) from PAAD-TCGA (The Cancer Genome Atlas) transcriptomic data. We then generated a heat-map of gene expression using the 'ComplexHeatmap' package. The ssGSEA (single sample Gene Set Enrichment Analysis) was used to evaluate the activities of the cancer-immunity cycle, which reflect the anti-tumor immune response and dictate the fate of cancer cells. Thereafter, we developed multiple algorithms to estimate the infiltration level of TIICs in the TME based on RNA sequencing (RNA-seq) data. We used six independent algorithms (TIMER, CIBERSORT-ABS, quanTIseq, xCell, TIP, and MCP-counter) to perform this calculaton with the aim of minimising calculation errors. Moreover, the effector genes of TIICs and 20 inhibitory immune checkpoints with therapeutic potential were also identified by the 'ComplexHeatmap' and 'Corrplot' packages, respectively. We also calculated a pan-cancer T-cell inflammation score [37], which is critical for determining the extent of cancer immunity and the ICB response, to estimate the correlation between these parameters and ZDHHC9 expression. The immunotherapy response was predicted by the Tumor Immune Syngeneic MOuse database (http://tismo.cistrome.org), TIDE database (http://tide.dfci.harvard.edu), and ROC Plotter (http://www.rocplot.org/) based on the

ZDHHC9 gene expression.

2.4. In vivo efficacy of ZDHHC9^{KD} and anti-PD-L1 in the Pan02-bearing tumor mouse model

The Pan02-bearing tumor mouse model was used to examine the in vivo efficacy of the *ZDHHC9*^{KD} and anti-PD-L1 combination therapy. After tumor implantation into C57BL/6 mice (as described above), two groups of mice received an intraperitoneal injection with anti-PD-L1 (BE0101) or an isotype control (immunoglobulin G2a [IgG2a]; BE0089) mAb at a dose of 100 μg per mouse in 100 μL InVivoPure pH 7.0 Dilution Buffer (Bio X Cell, Lebanon, NH, USA) (IP0070), every 3 days for a total of four cycles. Tumors were monitored and their size was recorded every 2–3 days. The tumor volume was calculated according to the following formula: $0.523 \times \text{length} \times \text{width}^2$. The efficacy of the combination therapy was evaluated by tumor imaging and tumor weight measurement.

We also established CD8$^+$-T-cell-depleted mice to investigate whether CD8$^+$ T cells were responsible for the anti-tumor effect of *ZDHHC9*^{KD} and anti-PD-L1 combination therapy. Briefly, C57BL/6 mice initially received 100 μg of the murine anti-CD8α antibody (BP0117) through intraperitoneal injection for a total of five cycles; the treatment was initiated on day 3 before tumor challenge and administered every 3 days (the treatment workflow is shown in Fig. 5e, i). The isotype control (IgG2b; BP0090) mAb was utilized as a negative control. Anti-PD-L1 was intraperitoneally administered after tumor implantation, as described above. Following the last injection, tumors were harvested for imaging and weighed. Next, the size of tumors was measured, and their volume was calculated according to the formula shown above. Tumor cells were further isolated and evaluated for their CD8$^+$ T cell composition (%). Simultaneously, tumor samples were frozen in liquid nitrogen, fixed in formalin, embedded in paraffin, and sliced into sections (thickness: 5 μm). Subsequently, the sections were stained with hematoxylin and eosin (H&E) and analyzed using immunohistochemistry (IHC).

2.5. Flow cytometry (FACS)

For the preparation of a single-cell suspensions, tumors were washed and digested in RPMI 1640 (Gibco), supplemented with 1000 U/mL collagenase type IV (Gibco) and 50 U/mL DNase I, for 30 min at 37 °C. Thereafter, the cells were filtered through 70 μm cell strainers (BD Falcon Cell Strainers; BD Biosciences, Oxford, U.K.). For surface markers staining, the cells were washed with cold PBS containing 2 % FBS and 2 mM ethylenediaminetetraacetic acid, harvested, and incubated with Fc Block (BD Biosciences) for 30 min. Next, the cells were stained with cell surface antibodies (Supplementary Table S1) in 50 μL of PBS (containing 1 % FBS and 2 mM ethylenediaminetetraacetic acid) at 4 °C for 1 h in the dark. After staining with surface antibodies, as described above, intracellular interferon-γ (IFN-γ) antibody staining was also performed. For IFN-γ staining, single tumor cells were treated with GolgiStop (BD Biosciences) and then stimulated with phorbol myristate acetate (100 ng/mL) and ionomycin (500 ng/mL) at 37 °C for 4 h. The tumor cells were then fixed and permeabilized with BD Fixation/Permeabilization solution (BD Biosciences, Franklin Lakes, NJ, USA). Finally, unstained and single-stained cells were subjected to FACS analysis. Data were collected using an Attune NxT flow cytometer (Thermo Fisher) and analyzed using the FlowJo software. All antibodies used for flow cytometry are listed in Supplementary Table S1.

2.6. Real-time quantitative polymerase chain reaction (RT-qPCR) and immunoblotting

RT-qPCR and immunoblotting were performed as previously described [38,39]. The following primer sequences were used for RT-qPCR: glyceraldehyde-3-phosphate dehydrogenase (GAPDH) (mouse), 5′-AGGTCGGTGTGAACGGATTTG-3′ (forward) and

5′-TGTAGACCATGTAGTTGAGGTCA-3′ (reverse); *ZDHHC9* (mouse), 5′-AAGGTGACACGGAAATGGGAG-3′ (forward) and 5′-CGACACTCG AAGGCAAAGAA-3′ (reverse). Antibodies against ZDHHC9 (HPA031814; Sigma Aldrich; USA) and β-actin (66009–1-Ig; Proteintech; China) were used for immunoblotting. Briefly, 5 × sodium dodecyl sulfate-polyacrylamide gel electrophoresis buffer was added to the samples, which were subsequently boiled at 95 °C for 10 min. Next, the samples were subjected to dodecyl sulfate-polyacrylamide gel electrophoresis on a 10 % gel and analyzed by immunoblotting with the indicated antibodies.

2.7. IHC and tissue microarrays (TMAs)

IHC analysis was performed as previously described [40]. Antibodies targeting granzyme B (GZMB; ab4059; Abcam), CD8α (98941S; Cell Signaling Technology), and Gr-1 (GB11229; Servicebio) were used for IHC. High-density protein TMAs of human pancreatic cancer clinical samples (catalog number PAC1602) were constructed by the Superbiotek Pharmaceutical Technology Co. Ltd. (Shanghai, China). PAAD TMA slides were heated and dewaxed. The antigen was subsequently retrieved and incubated with an anti-ZDHHC9 antibody. A signal was obtained via the labeled streptavidin-biotin method. The staining intensity of anti-ZDHHC9 antibody. A total of 80 TMAs were classified into four groups: weak staining was marked as 1; faint staining as 2; moderate staining as 3; and strong staining as 4. The degree of immunostaining was examined and blindly scored in a blinded manner by two independent pathologists. The scores were assigned according to the percentage of stained cells and staining intensity.

2.8. Cytokine analysis

The secretion of cytokines by tumors was measured using the enzyme-linked immunosorbent assay (ELISA) and the cytometric bead array (CBA). The ELISA was performed as previously described [41]. A commercial BD™ CBA mouse Th1/Th2/Th17 cytokine kit (BD Biosciences) was used to detect the level of cytokines in tumor plasma. The specific experimental procedures were consistent with our previous study [42]. According to the assay protocol, dissociated tumor cells were centrifuged to collect tumor plasma samples for further detection on a BD Accuri™ C6 Plus flow cytometer (BD Biosciences, Franklin Lakes, NJ, USA). Briefly, a vial of lyophilized cytokine standards was prepared in assay diluent and serially diluted. Mixed cytokine capture beads were then incubated with tumor plasma samples, standards, and the negative control for 30 min at room temperature in the dark. The assay was subsequently performed on a BD Accuri™ C6 flow cytometer, and the data were analyzed using the BD FCAP Array software (BD Biosciences).

2.9. Synthesis and physicochemical characterization of NP-siZDHHC9

We used the double emulsion solvent evaporation technique to prepare siZDHHC9-encapsulating polymeric NPs as previously described [43]. siRNA targeting mZDHHC9 and siRNA negative control (siNC) were synthesized by Beijing TSINGKE Biological Technology Co. Ltd. The sequences of si*ZDHHC9* were: sense strand, 5′-CAACCA-GAUUGUGAAACUGAA-3′, antisense strand, 5′-UUCAGUUUCACAAU-CUGGUUG-3′. The sequences of si*NC* were: sense strand, 5′-CCUUGAGGCAUACUUCAAAdTdT-3′, antisense strand, 5′-UUU-GAAGUAUGCCUCAAGGdTdT-3′. Briefly, an aqueous solution containing 10 µg of siRNA (si*ZDHHC9*, si*NC*, or 5′-carboxyfluorescein-labelled [FAM-labelled] si*NC*) in 25 µL of BeyoPure™ Ultrapure water (Beyotime) was emulsified in 0.5 mL of chloroform solution (containing a cationic molecule DOTAP and a copolymer of mPEG-PLGA at 2 mg/mL and 50 mg/mL, respectively) by sonicating for 1 min. Next, this primary emulsion was rapidly added dropwise to a tube containing 5 mL of Ultrapure water, and another round of sonication for 1 min was performed at 4 °C. This led to the instant formation of siRNA-loaded NPs (NP-siRNA) in a water-in-oil-in-water emulsion. The NPs were subsequently collected using a rotary evaporator (EyeLaN; Tokyo Rikakikai Co., Ltd., Tokyo, Japan) under reduced pressure to remove the solvent (chloroform and Ultrapure water). The sample was concentrated to a volume of 1 mL, and the NP-siRNA was filtered and stored at – 80 °C. The average hydrodynamic size, polydispersity index, and zeta potential of the NP-siRNA complexes were determined via dynamic light scattering (Malvern Zetasizer). The morphology of NP-siRNA was also determined by transmission electron microscopy (TEM; JOEL, Japan). For TEM, the NP-siRNA was initially stained with 2 % uranyl acetate and air dried on a Formvar/Carbon film grid (Electron Microscopy Sciences, Hatfield, PA, USA).

2.10. Cellular uptake and transfection with NP-siZDHHC9 in vitro

FAM-labelled si*NC*-loaded NPs (NP-FAM-si*NC*) were prepared to monitor the uptake of NPs. A total of 2×10^5 Pan02 cells per well were seeded in a six-well plate containing 2 mL of RPMI 1640 medium and incubated at 37 °C overnight. Subsequently, the cells were incubated with medium containing NP-FAM-si*NC* for 6 h, washed with Dulbecco's PBS and analyzed on a BD Accuri™ C6 Plus flow cytometer. To confirm that the transfection with FAM-labelled siNC was successful, the cells were treated with NP-FAM-si*NC* for 6 h, prior to incubated with Lyso-Tracker™ Deep Red (1:20,000, Invitrogen; CA, USA) and observed on a Zeiss LSM 880 confocal laser scanning microscope. The Pan02 cells were transfected with the NP-si*ZDHHC9* complexes to evaluate their in vitro gene silencing efficacy by RT-qPCR.

### 2.11. Cell proliferation assay and in vitro cytotoxicity

The Cell Counting Kit-8 (CCK-8) assay (Dojindo, Kumamoto, Japan) was utilized to determine the viability of cells in the proliferation and cell cytotoxicity assays. For the in vitro cell cytotoxicity assay, 2×10^3 cancer cells per well were seeded in 96-well plates containing the corresponding culture medium. The following day, cells were treated with fresh medium containing PBS, naked siRNA, or NP siRNA at indicated concentrations. After incubation for 48 h, 100 µL Cell Counting Kit (CCK-8) reagent was added to each well, and the cells were incubated for a further 1.5 h in the dark at 37 °C. The optical density (OD) was measured at 450 nm wavelength using the Spectra Max M5 microplate reader (Molecular Devices, Sunnyvale, CA, USA). The cell viability rate was calculated according to the following formula: Cell viability (%) = $(OD_{treated} - OD_{blank}) / (OD_{control} - OD_{blank}) \times 100$ %.

2.12. In vivo efficacy of the NP-siZDHHC9 and anti-PD-L1 combination therapy in Pan02- and KPC-bearing tumor mouse models

Pan02- and KPC-bearing tumor mouse models were developed to evaluate the combined therapeutic efficacy of NP-si*ZDHHC9* and anti-PD-L1. Wild-type cells (Pan02, 5×10^6; KPC, 3×10^6) suspended in 100 µL of PBS were injected into the right flank of male C57BL/6 mice at 6 weeks of age. After tumor implantation 10–12 days, the mice were randomly divided into five groups (n = 8 or 9 mice/group). Each group of mice received intratumoral injection with saline (50 µL), NP-si*NC*, or NP-si*ZDHHC9* (final siRNA concentration: 0.8 mg/kg body weight) every 3 days. Mice in the 'anti-PD-L1' and 'NP-si*ZDHHC9* plus anti-PD-L1' groups received an additional intraperitoneal injection with anti-PD-L1 mAb (100 µg per mouse). The treatment scheme is shown in Fig. 3j and o. Tumor size was monitored using an electronic caliper (Mitutoyo, Mississauga, Canada) and calculated according to the formula mentioned above. After the experiments, the tumors were harvested for FACS, RT-qPCR, IHC, and ELISA analyses.

2.13. Statistical analysis

All experiments were independently performed in triplicate, and the
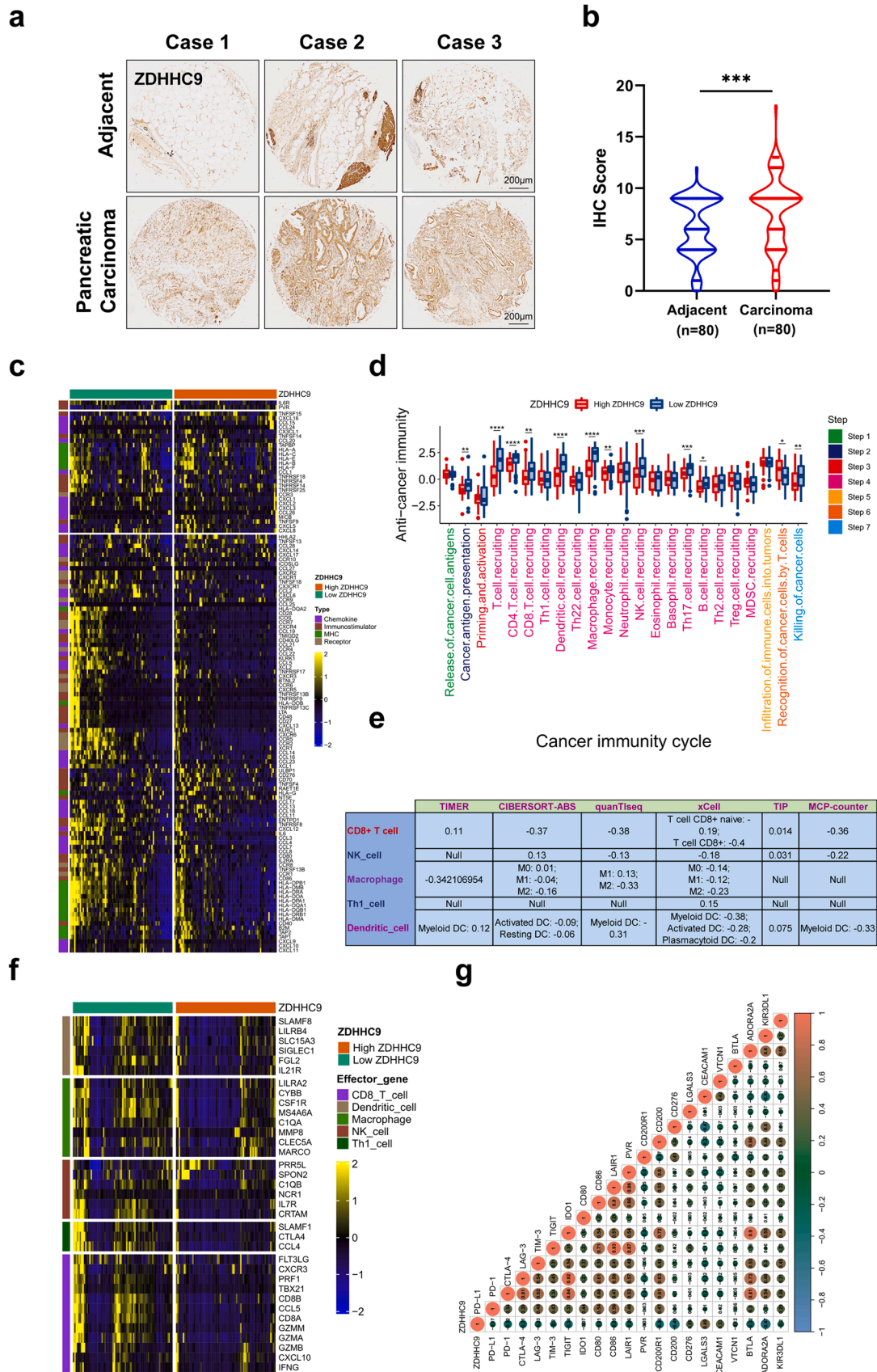
(caption on next page)

Fig. 1. ZDHHC9 was highly expressed in pancreatic cancer and promoted an immunosuppressive TME. (a) IHC analysis of ZDHHC9 using microarrays of human normal pancreatic tissues and pancreatic cancer tissues. (b) Violin plot of ZDHHC9 expression in tissue sections based on the IHC score recorded by the IHC score obtained by pathologists (n = 80 normal pancreatic specimens, n = 80 pancreatic cancer specimens, $p = 0.003$, t(2) = 3.821, df = 79) tissue sections; scale bars = 200 μm. (c) Differential expression heat map of published immunomodulators (chemokines or their receptors, MHC molecules, and immune stimulators) between high- and low-*ZDHHC9* groups in patients with PAAD. (d) Different expression patterns of the various steps of the cancer-immunity cycle between the high- and low-*ZDHHC9* groups. (e) Correlation analysis between the expression of *ZDHHC9* and the infiltration levels of five types of TIICs (i.e., CD8$^+$ T cells, NK cells, macrophages, Th1 cells, and DCs), according to six independent algorithms. (f) Differential expression heat map of the effector genes in the above-mentioned tumor-associated immune cells between the high- and low-*ZDHHC9* groups. (g) Correlation between the expression of *ZDHHC9* and 20 inhibitory immune checkpoints. The color scales and the values represent the Spearman correlation coefficient. The clustered heat map depicts the mRNA expression z-scores relative to all samples. (b) *p*-value was calculated using paired Student's t-test; (d) *p*-values were calculated using Mann-Whitney U test with asterisks indicating statistical significance (*$p < 0.05$, **$p < 0.01$, *** $p < 0.001$, and ****$p < 0.0001$).

data are shown as mean ± standard deviation (SD) or mean ± standard error of the mean (SEM) (n ≥ 3), as indicated. The statistical analyses were carried out using one-way analysis of variance (ANOVA) with Tukey's correction (for comparisons between more than three groups) and Student's t-test or Mann Whitney U test (for comparisons between two groups). GraphPad Prism (Version 8.0; GraphPad Software Inc., San Diego, CA, USA) and SPSS (Version 23.0; IBM Corp., Armonk, NY, USA) statistical software were used to perform the analyses; *p*-values < 0.05 denoted statistically significant differences.

3. Results

3.1. ZDHHC9 was frequently overexpressed in numerous human cancers, including pancreatic cancer

To analyze the clinical relevance of ZDHHC9 in human cancers, we investigated its expression status across numerous types of cancer using RNA-sequencing data from The Cancer Genome Atlas (TCGA) and the Gene Expression Profiling Interactive Analysis (GEPIA) platform [44]. We found that *ZDHHC9* mRNA expression was significantly increased in 20 of the 33 most common types of human cancer (Fig. S1a, b). In 29 types of human cancer, we observed a negative correlation between *ZDHHC9* expression and the immune infiltration score (Fig. S1c and S2). We further evaluated the correlation between *ZDHHC9* expression and the 18 signature genes of existing adaptive T cell immune responses [37]. The results showed that ZDHHC9 expression was negatively correlated with the pro-inflammatory T cell gene signature, as well as the immune cell cytotoxicity gene signature (i.e., granzyme A [*GZMA*] and perforin 1 [*PRF1*]) [45] (Fig. S1d, e). Additionally, the elevated expression of *ZDHHC9* was associated with poor prognosis in several cancer types (Fig. S3), including pancreatic cancer. Pan-cancer analysis indicated that *ZDHHC9* expression was negatively correlated with most immunomodulators (i.e., chemokines, major histocompatibility complex [MHC] molecules, immune stimulators, and receptors) and tumor-infiltrating immune cells (TIICs) in a variety of human cancers from the TISIDB database (Fig. S4a) [46]. Numerous studies have demonstrated the low expression of immune checkpoints such as PD-L1/PD-1 in the immunosuppressive TME [47,48]. Notably, the expression of *ZDHHC9* and several immune checkpoints, such as *PD-L1*, cytotoxic T-lymphocyte associated protein 4 (*CTLA-4*), and lymphocyte activating 3 (*LAG-3*), was largely mutually exclusive (Fig. S4b, c). A positive correlation was found between MDSC infiltration and *ZDHHC9* expression, whereas a negative correlation was observed between CD8$^+$ T cells and *ZDHHC9* expression in multiple human cancers (Fig. S5a, b). Taken together, our data indicate that *ZDHHC9* was frequently upregulated in human cancers, including pancreatic cancer. However, the biological role and underlying mechanism of the ZDHHC9 in pancreatic cancer have not previously been reported.

3.2. ZDHHC9 was highly expressed in pancreatic cancer and correlates with impaired anti-tumor immunity

We next explored the expression of ZDHHC9 by IHC in a TMA containing 80 cancerous and normal pancreatic tissues. As shown in Fig. 1a

and b, the protein expression levels of ZDHHC9 were markedly higher in cancer tissues versus normal pancreatic tissues. To further examine the critical role of ZDHHC9, we explored its connection with immunity-related factors in pancreatic cancer using data from the TCGA database ZDHHC9 expression was found to be negatively correlated with a large number of immunomodulators (Fig. 1c), the genetic signature of the pro-inflammatory TME [49]. Anti-tumor immune response involves a series of stepwise events. This advance provides an opportunity for dissecting the complex interactions between cancer and the immune system [50]. We further uncovered potential steps of the cancer-immune cycle that were influenced by ZDHHC9 in PAAD. The activities of the majority of these cancer-immune cycle steps were downregulated in the *ZDHHC9*-high expression group, including cancer antigen presentation (Step 2), immune cell recruitment (Step 4), and cytotoxicity against cancer cells (Step 7; Fig. 1d). Of note, Step 4 involved the recruitment of CD4$^+$ T cells, CD8$^+$ T cells, dendritic cells (DCs), macrophages, monocytes, natural killer (NK) cells, T helper type 17 (Th17) cells, and B cells. Thus, the reduced activities of these cancer-immune cycle steps may suppress the anti-tumor immune response and reduce the infiltration of effector TIICs into the TME. We further calculated the infiltration of TIICs into the TME using six independent algorithms in PAAD. In line with the above results, *ZDHHC9* was negatively correlated with the infiltration of CD8$^+$ T cells, NK cells, and macrophages (Fig. 1e). Similarly, *ZDHHC9* was negatively correlated with the effector genes of these TIICs (Fig. 1f). Moreover, *ZDHHC9* was also negatively correlated with the majority of immune checkpoint inhibitors including *PD-L1*, *PD-1*, *CTLA-4*, *LAG-3*, T cell immunoglobulin and mucin-domain-containing molecule 3 (*TIM-3*), T cell immunoglobulin and immunoreceptor tyrosine-based inhibitory motif domain (*TIGIT*), and adenosine 2A receptor (*ADORA2A*) (Fig. 1g). The mutation profiles of high- and low-*ZDHHC9* tumors revealed that *KRAS* and dynein axonemal heavy chain 11 (*DNAH11*) were among the most differentially mutated genes (Fig. S6a, b). *KRAS* mutations are associated with an immunosuppressive pancreatic cancer microenvironment [51]. *ZDHHC9*-high tumors had a higher frequency of *KRAS* mutations compared with *ZDHHC9*-low tumors. Similarly, tumors containing *KRAS* mutations were more likely to be *ZDHHC9*-high (64 %, 49/77) compared with wild-type *KRAS* tumors (37 %, 24/65) (Fig. S6c). Moreover, *ZDHHC9* was positively correlated with genes upregulated as a result of *KRAS* mutation. In contrast, it was negatively correlated with genes downregulated due to the *KRAS* mutation (Fig. S6d, e). Collectively, these findings led us to propose that ZDHHC9 expression promoted an immunosuppressive or 'cold' TME in pancreatic cancer.

3.3. ZDHHC9 deficiency significantly induced tumor regression and prolonged the survival time of mice with transplantable pancreatic tumors

To further assess whether ZDHHC9 represents a potential therapeutic target in pancreatic cancer, we initially examined the effect of targeting ZDHHC9 on tumor growth and weight in different tumor models. We achieved *ZDHHC9* KD by stably transfecting Pan02 cells with an expression vector encoding one of three shRNA targeting *ZDHHC9* or the shControl. We confirmed the efficacy of *ZDHHC9* KD by RT-qPCR and immunoblotting analyses (Fig. S7a, b), which revealed
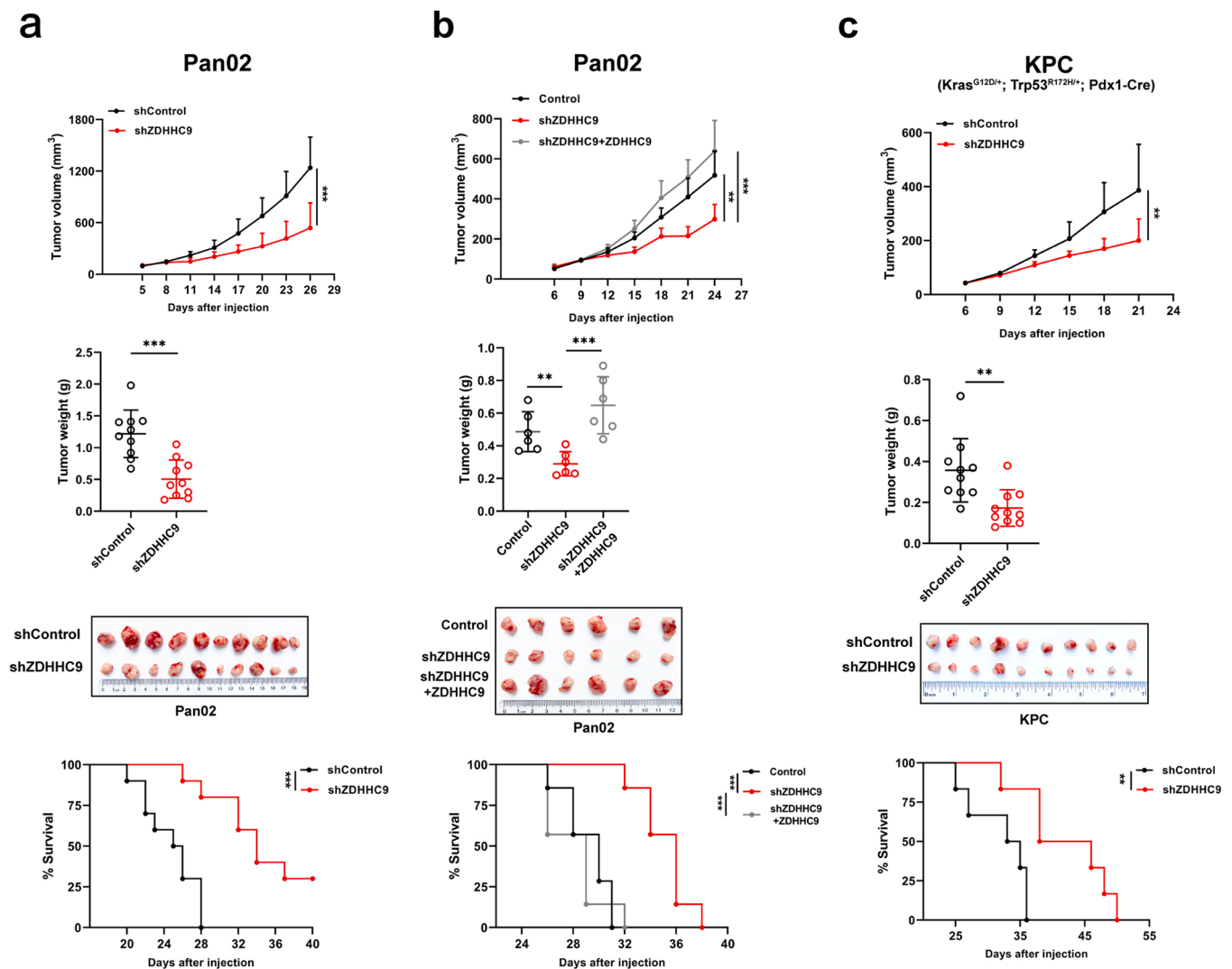
Fig. 2. Targeting ZDHHC9 decreased tumor growth and prolonged survival in pancreatic tumor models. (a) Curves of subcutaneous tumor growth in the right flank of syngeneic mice that received 5×10^6 Pan02 cells stably expressing sh*ZDHHC9* or shControl vector Pan02 subclones ($n = 10$ mice per group; tumor volume ($p = 0.0001$, t(2) = 4.820, df = 18); tumor weight ($p = 0.0002$, t(2) = 4.708, df = 18); survival rate ($p = 0.0002$, Chi square = 14.36, df = 1). The tumor volume, tumor weight, representative images of shControl and sh*ZDHHC9* Pan02 tumors at the end of the experiment, and survival curves of shControl or sh*ZDHHC9* Pan02 tumors are shown ($n = 10$ mice per group). (b) Subcutaneous tumor growth in syngeneic mice that received 2×10^6 Pan02 subclones stably expressing the Control, sh*ZDHHC9*, or (sh*ZDHHC9*+*ZDHHC9*) constructs ($n = 6$ mice per group). Growth curves, tumor weight, representative images of the tumors, and mice survival curves are shown (tumor volume (sh*ZDHHC9* vs sh*ZDHHC9*+Flag-ZDHHC9: $p = 0.0003$, q = 7.332, df = 15); tumor weight (sh*ZDHHC9* vs sh*ZDHHC9*+Flag-ZDHHC9: $p = 0.0003$, q = 7.418, df = 15); survival rate ($p = 0.0002$, Chi square = 16.88, df = 2). (c) Growth curves, tumors weight, representative images of the tumors, and survival curves for the mice bearing shControl or sh*ZDHHC9* KPC tumors ($n = 10$ mice per group; tumor volume ($p = 0.0059$, t(2) = 3.124, df = 18); tumor weight ($p = 0.0044$, t(2) = 3.257, df = 18); survival rate ($p = 0.0092$, Chi square = 6.793, df = 1). Survival curves from the subcutaneous tumor model were determined until death or a tumor volume > 1000 mm³. Tumor-bearing mice were euthanized when the calculated tumor volume ~2000 mm³ or when tumors became necrotic. All results are presented as mean ± SD. (a and c) *p*-values were calculated using a two-sided unpaired Student's t-test; (b) *p*-values were calculated using a one-way ANOVA with a Tukey post hoc test. Survival curves were analyzed using the log-rank (Mantel-Cox) test (** $p < 0.01$, and *** $p < 0.001$).

almost complete *ZDHHC9* KD in the sh*ZDHHC9*#1 Pan02 subclones. We next established the critical role of *ZDHHC9* KD in tumor progression using a subcutaneous mouse model of pancreatic cancer (by transplanting Pan02 cells). We subcutaneously injected 5×10^6 parental or Pan02-*ZDHHC9*^KD cells into the right flank of immunocompetent C57BL/6 mice and monitored tumor growth every 2–3 days. Mice lack of survival was defined as death or a tumor size >1000 mm³. Notably, *ZDHHC9*^KD in Pan02 cells dramatically impaired tumorigenesis, as evidenced by the smaller tumor size, lower tumor weight, and prolonged survival time of the animals (Fig. 2a). To further confirm the specificity of *ZDHHC9*^KD on tumor progression, overexpression of ZDHHC9 in Pan02-*ZDHHC9*^KD cells reversed the inhibitory effect on tumor growth, confirming the on-target anti-tumor effect of *ZDHHC9*^KD (Fig. 2b,

Fig. S7c).

We further assessed whether ZDHHC9 deficiency in tumor cells could exert a similar tumor suppressive effect on different molecular subtypes of pancreatic cancer. For this purpose, we tested the therapeutic potential of *ZDHHC9* KD using an additional syngeneic mouse subcutaneous KPC tumor model: (*LSL-Kras*^G12D/+; *LSL-Trp53*^R172H/+; and *Pdx1-Cre*) derived cell line KPC (with two mutations confirmed by PCR analysis) (Fig. S7d, e) [17]. The efficiency of stable shRNA-mediated *ZDHHC9* KD was validated by RT-PCR and immunoblotting analyses in the KPC cells (Fig. S7f, g). In the KPC subcutaneous tumor model, we subcutaneously inoculated 3×10^6 parental or KPC-*ZDHHC9*^KD cells into the right flank of immunocompetent C57BL/6 mice as described above. We found that the tumor inhibition rate was 51.5 % with a
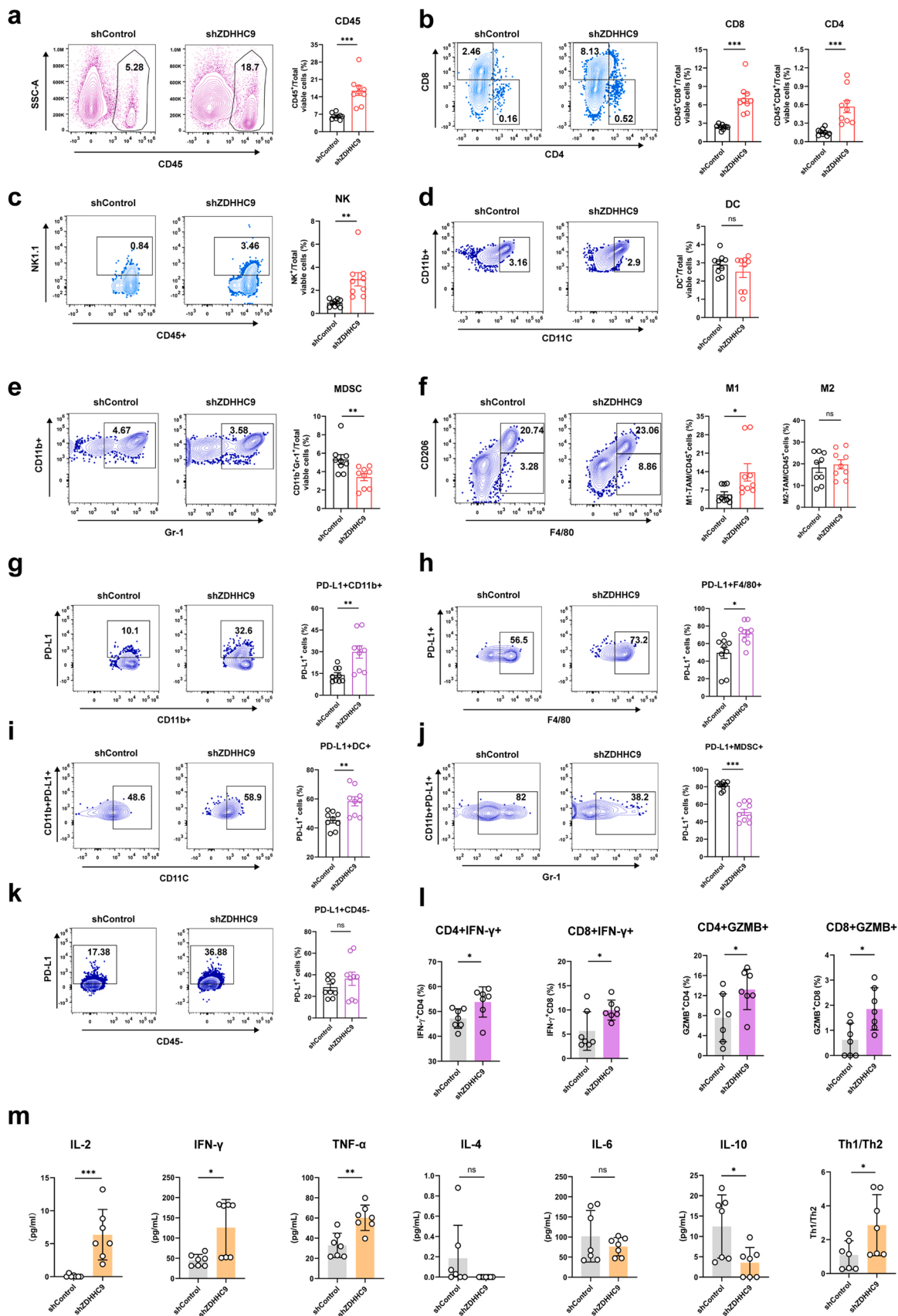
(caption on next page)

Fig. 3. Loss of ZDHHC9 induced a pro-inflammatory TME by enhancing the infiltration of anti-tumor immune effector cells and increasing tumor inflammation. (a-f) Flow cytometry analysis of the number of CD45$^+$ leukocytes (a) ($p < 0.0001$, t(2) = 5.245, df = 16), CD8$^+$ T cells (CD8) ($p < 0.0001$, t(2) = 5.693, df = 16), CD4$^+$ T cells (CD4) ($p = 0.0007$, t(2) = 4.210, df = 16) (b), NK cells (NK) ($p = 0.0028$, t(2) = 3.527, df = 16) (c), DCs ($p = 0.3047$, t(2) = 1.061, df = 16) (d), CD11b$^+$ Gr-1$^+$ myeloid-derived suppressor cells (MDSCs) ($p = 0.0091$, t(2) = 2.966, df = 16) (e), type 1 macrophages (M1) ($p = 0.0277$, t(2) = 2.422, df = 16), and type 2 macrophages (M2) ($p = 0.6547$, t(2) = 0.4558, df = 16) (f) infiltrating subcutaneous tumors, namely shControl and sh*ZDHHC9* Pan02 tumors. The percentages indicate different immune cell populations as proportion of the total live cells, except for macrophages, where percentages indicate the percentage of total live CD45$^+$ cells. The results are presented as mean ± SEM. (g-k) Flow cytometric analysis and the quantitative results of PD-L1$^+$ (CD11b: $p = 0.0032$, t(2) = 3.471, df = 16), (F4/80: $p = 0.0102$, t(2) = 2.913, df = 16), (DCs: $p = 0.003$, t(2) = 3.496, df = 16), (MDSCs: $p < 0.0001$, t(2) = 7.909, df = 16), (CD45-: $p = 0.2671$, t(2) = 1.150, df = 16) cells in Pan02 tumors. (i) Frequencies of IFN-γ^+- or GZMB$^+$-producing CD4$^+$ and CD8$^+$ T cells on day 26 after injection with shControl and sh*ZDHHC9* Pan02 tumors ($n = 7$ mice per group; IFN-γ^+CD4: $p = 0.0317$, t(2) = 2.431, df = 12; IFN-γ^+CD8: $p = 0.0255$, t(2) = 2.549, df = 12; GZMB$^+$CD4: $p = 0.0337$, t(2) = 2.397, df = 12; GZMB$^+$CD8: $p = 0.0103$, t(2) = 3.039, df = 12). (m) Concentrations of IL-2, IFN-γ, TNF-α, IL-4, IL-6, IL-10, and IL-17 in the supernatant of excised tumors from the indicated mice using a Th1/Th2/Th17 cytometric bead array (CBA) kit ($n = 7$ mice per group; $p = 0.03647$, t(2) = 2.354, df = 12); (a-m) *p*-values were analyzed using a two-sided unpaired Student's t-test. All results are presented as mean ± SD (*ns* = not significant, **p* < 0.05, ** *p* < 0.01, and ***p* < 0.001).

significant improvement in the survival of tumor-bearing mice (Fig. 2c). In summary, KD of ZDHHC9 in pancreatic tumor cells could significantly induce pancreatic tumor regression and prolong the survival time of mice.

3.4. ZDHHC9 inhibition induced a pro-inflammatory TME with characteristic anti-tumor immune profiles

To understand the mechanism through which *ZDHHC9* KD mediated anti-tumor effects, we examined the overall immune landscape by focusing specifically on TME remodelling. The alterations of immune cell subsets in *ZDHHC9*^{KD} tumors were characterized using multispectral flow cytometry. The gating strategies for immune cell subsets are shown in Fig. S8. *ZDHHC9* KD in Pan02 tumors significantly increased the proportion of live CD45$^+$ cells, NK cells, CD8$^+$ T cells, CD4$^+$ T cells, and M1 macrophages at the tumor site; however, it did not affect the recruitment of M2 macrophages. MDSCs play essential roles in the suppression of host immune responses, and their accumulation at the tumor site maintains the immunosuppressive TME [52]. The results revealed that the infiltration of CD11b$^+$Gr-1$^+$ MDSCs decreased in *ZDHHC9*^{KD} Pan02 tumors. There was no significant difference in the percentages of DCs, as determined by FACS staining for relevant cell surface markers (Fig. 3a-f). Strikingly, in the *ZDHHC9*^{KD} Pan02 tumors, intratumoral NK cells and CD8$^+$ T cells exhibited a reduction in PD-1 expression (a marker of exhaustion), compared with untreated tumors. In addition, the expression of PD-1 on CD4$^+$ T cells was not significantly changed in *ZDHHC9*^{KD} Pan02 tumors (Fig. S9a-c). These findings support the view that, in Pan02 tumors, *ZDHHC9*^{KD} boosted the cellular immune response and delayed effector T-cell exhaustion. *ZDHHC9* KD in the tumor reprogrammed the TME in favor of the anti-tumor immune landscape. We observed that *ZDHHC9* KD improved T cell infiltration and function. In addition, it also increased the expression of the PD-L1 checkpoint molecule on CD11b$^+$ myeloid cells, F4/80$^+$ macrophages, and DCs (Fig. 3g-k).

The crosstalk between tumor and immune cells within the TME relies primarily on cytokine and chemokine signalling, which drives and determines tumor progression [53]. Therefore, we next evaluated the cytokine and chemokine milieu within the ZDHHC9-deficient TME. We examined the T-cell-mediated production of IFN-γ and GZMB in subcutaneously grown shControl and sh*ZDHHC9* Pan02 tumors. The results demonstrated that tumor-infiltrating CD8$^+$ T cells and CD4$^+$ T cells from the sh*ZDHHC9* group exhibited higher IFN-γ and GZMB production than those of the shControl group (Fig. 3l; Fig. S10a-d). These findings suggest that the activation of functional CD8$^+$ and CD4$^+$ effector T cells was achieved by *ZDHHC9* KD. We further investigated the concentrations of Th1- and Th2-related cytokines in the tumors using a mouse Th1/Th2/Th17 CBA kit. We detected increased levels of the Th1 pro-inflammatory cytokines interleukin 2 (IL-2), IFN-γ, and tumor necrosis factor alpha (TNF-α), as well as a decreased levels of IL-10 in *ZDHHC9*^{KD} tumors, compared with the control group; there were no changes in the levels of IL-4 and IL-6. In addition, we did not detect significant levels of IL-17 in tumor tissues (data not shown). The raised

Th1/Th2 cytokine ratio indicates that *ZDHHC9* KD in the tumor increased the local pro-inflammatory response (Fig. 3m). Chemokines play an essential role in driving T cell trafficking, thus regulating the immune response and homeostasis [54]. Indeed, we observed that *ZDHHC9* KD in tumors increased the plasma concentrations of C-C motif chemokine ligand 5 (CCL5), C-X-C motif chemokine ligand 10 (CXCL10), CXCL9, and IFN-γ within the TME (Fig. S11a). Previous research showed that such a chemokine signature was correlated with the infiltration of CD8$^+$ T cells in PAAD [55]. Of note, all these inflammation-related chemokine and cytokine profiles were observed only within the locality of the tumor, but not in the blood (Fig. S11b). This, indicates that the increased production of CCL5, CXCL10, CXCL9, and IFN-γ may have originated from the tumor site with minimal systemic effects. Taken together, these results establish a critical role of tumoral ZDHHC9 in the regulation of the composition and activation of the cellular immune response at the tumor site. The increased T-cell infiltration into the tumor, as well as the localized release of pro-inflammatory chemokines and cytokines, serve to create a pro-inflammatory TME. In summary, our data indicated that ZDHHC9 deficiency improves anti-tumor immunogenicity and may strongly synergize with anti-PD-L1 checkpoint therapy, thereby resulting in significant tumor regression.

3.5. Combination therapy with anti-PD-L1 and ZDHHC9 deficiency overcome tumor resistance to PD-L1 blockade therapy

As described above, *ZDHHC9* KD improved T cell infiltration and function but also upregulated the expression of the PD-L1 checkpoint molecule on CD11b$^+$ myeloid cells, F4/80$^+$ macrophages, and DCs. For this purpose, we hypothesized that *ZDHHC9* KD may enhance the therapeutic efficacy of PD-L1 blockade therapy. We next tested the synergistic therapeutic effect of ZDHHC9 inhibition and PD-L1 blockade in poorly immunogenic tumor models. We constructed transplantable Pan02 tumor models with primary resistance to anti-PD-L1 therapy [56, 57]. An anti-PD-L1 monoclonal mAb or an isotype control (IgG2a) were intraperitoneally administered twice per week to C57BL/6 mice after subcutaneous transplantation of 2×10^6 parental or Pan02-*ZDHHC9*^{KD} cells. The use of anti-PD-L1 alone led to a modest inhibition of tumor growth. Nevertheless, the combination treatment with *ZDHHC9* KD and anti-PD-L1 markedly inhibited tumor growth and prolonged the survival time of Pan02 tumor-bearing mice compared with *ZDHHC9* KD or anti-PD-L1 mAb treatment alone (Fig. 4a-e). Importantly, the combination therapy was well tolerated and did not result in acute toxicity, as evidenced by the lack of reduction in body weight (Fig. S12). Taken together, the inhibition of both ZDHHC9 and PD-L1 functions synergistically retarded tumor growth in the pancreatic tumor xenograft model.

3.6. The host immune system mediated the synergistic effect of ZDHHC9 deficiency and anti-PD-L1 therapy

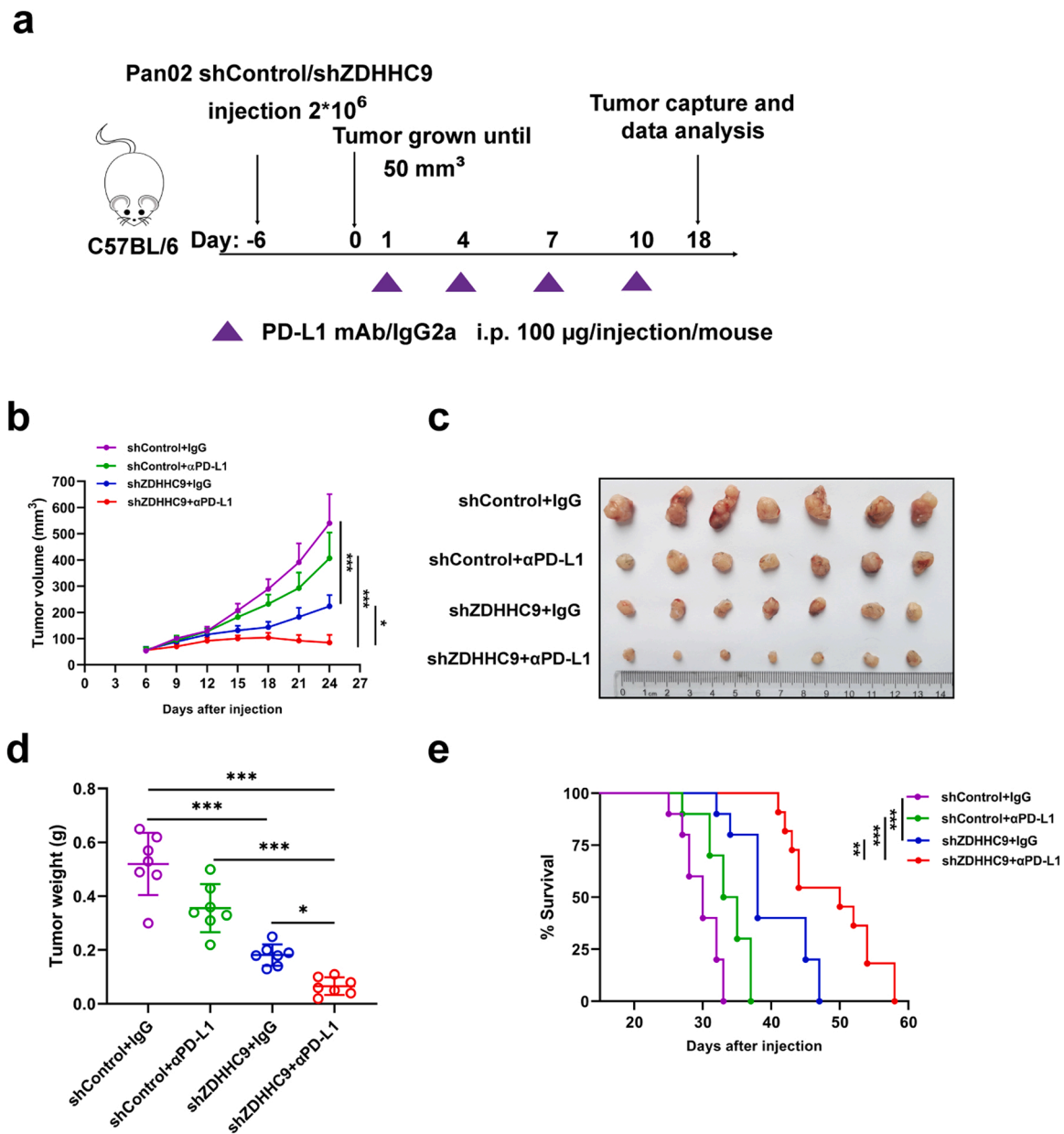Based on the above results, we hypothesized that the host immune

Fig. 4. Inhibition of ZDHHC9 potentiated anti-PD-L1 mAb treatment to induce robust anti-tumor immunity. (a-d) C57BL/6 mice were subcutaneously injected with shControl or sh*ZDHHC9* Pan02 cells and treated with an anti-PD-L1 mAb or an IgG control. Scheme of treatment (a), tumor growth curves (b; p(shControl+IgG vs sh*ZDHHC9*+IgG)< 0.0001, q = 10.71; p(shControl+IgG vs *ZDHHC9*+αPD-L1)< 0.0001, q = 15.39; p(sh*ZDHHC9*+IgG vs sh*ZDHHC9*+αPD-L1) = 0.0146, q = 4.679); representative tumor images (c), and tumor weight (d; p(shControl+IgG vs sh*ZDHHC9*+IgG)< 0.0001, q = 11.56; p(shControl+IgG vs sh*ZDHHC9*+αPD-L1)< 0.0001, q = 15.52; p(shControl+αPD-L1 vs sh*ZDHHC9*+αPD-L1) < 0.0001, q = 9.904; p(sh*ZDHHC9*+IgG vs sh*ZDHHC9*+αPD-L1) = 0.0463, q = 3.952) for tumor-bearing mice (n = 7 mice per group). Survival curves of tumor-bearing mice from each group after the indicated treatment (e) (n = 10 mice per group, p(shControl+IgG vs sh*ZDHHC9*+IgG)< 0.0001, Chi square = 17.38; p(shControl+αPD-L1 vs sh*ZDHHC9*+αPD-L1)< 0.0001, Chi square = 21.70; p(sh*ZDHHC9*+IgG vs sh*ZDHHC9*+αPD-L1) = 0.0093, q = 6.772). All results are presented as mean ± SD. (b and d) The p-values were calculated using a one-way ANOVA with a Tukey post hoc test. (e) Survival curves of the groups were analyzed using the log-rank (Mantel-Cox) test (*$p < 0.05$, **$p < 0.01$, and ***$p < 0.001$).

system mediated the anti-tumor activity that arises from ZDHHC9 depletion in the tumor site. To test this hypothesis, we established a subcutaneous transplantation mouse model using NOG mice that constitutively lacked T, B, and NK cell activities. These mice were subcutaneously inoculated with parental or Pan02-*ZDHHC9*[KD] cells. Notably, after 26 days, there was no significant difference between the Control and *ZDHHC9*[KD] groups. More importantly, *ZDHHC9* KD in Pan02 cells resulted in a ~55 % inhibition of the tumor growth rate following the inoculation of immunocompetent C57BL/6 mice with the cells. However, the depletion of ZDHHC9 in Pan02 cells only caused a ~14 % reduction of the tumor growth rate in NOG mice (Fig. 5a-d),

indicating that the anti-tumor effect of ZDHHC9 deficiency largely depends on the presence of an intact immune system. Besides, A small part of the tumor inhibitory effect mediated by ZDHHC9 also attributed from the capacity to inhibit proliferation of tumor cells. To identify specific types of immune effector cells linked to the anti-tumor activity of ZDHHC9 deficiency, we used a CD8-neutralizing antibody to block CD8^{+} T cells in C57BL/6 mice bearing control and *ZDHHC9*[KD] Pan02 tumors. Mice were intraperitoneally injected with a neutralizing CD8 antibody or an IgG2b isotype control, twice per week (Fig. 5e) [57]. Treatment with an anti-CD8 antibody reduced the total number of CD8^{+} T cells in the tumors and spleens of mice, as confirmed by flow
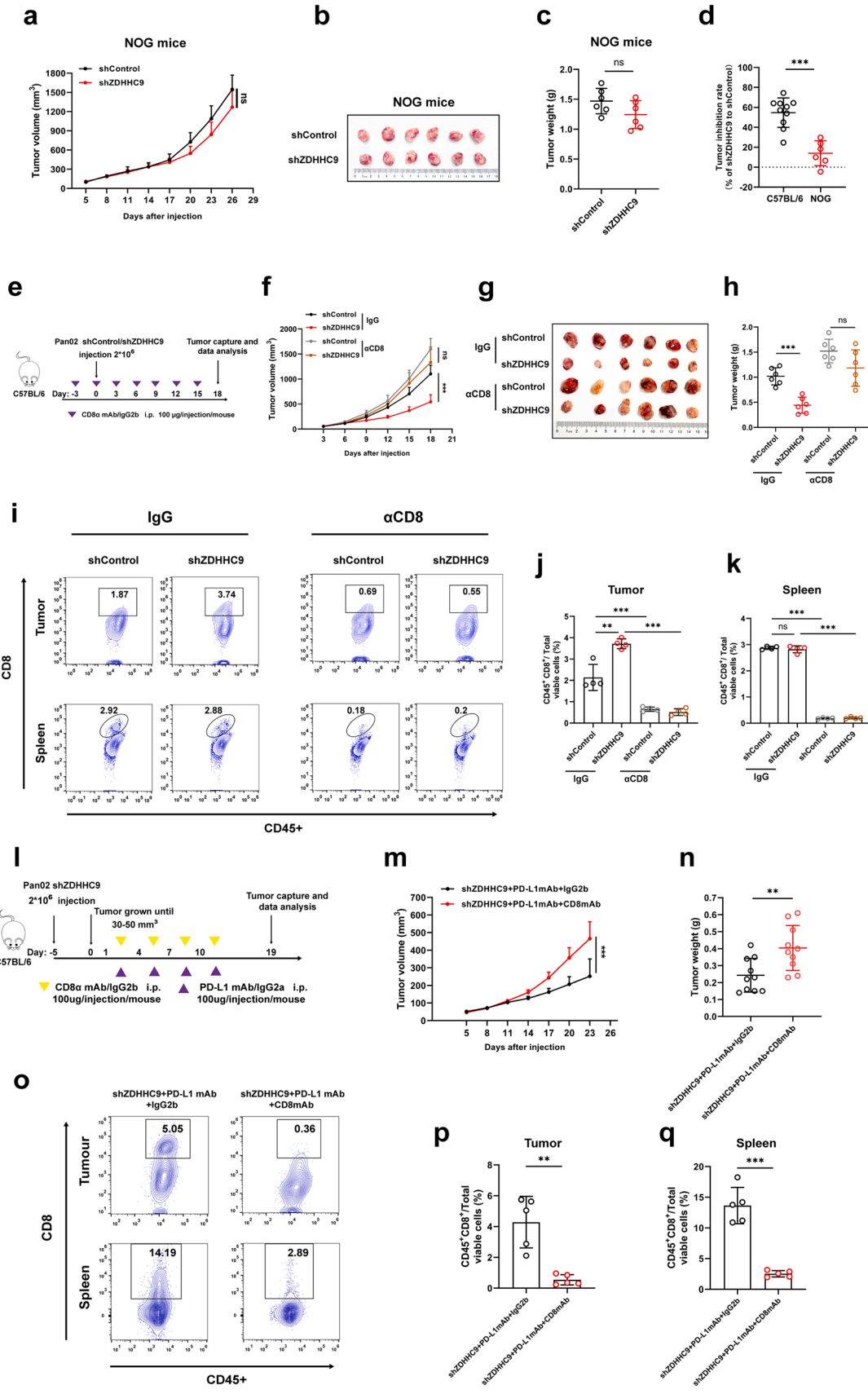
(caption on next page)

Fig. 5. The synergistic effect of combining anti-PD-L1 mAb treatment and ZDHHC9 inhibition was largely mediated by CD8$^+$ T cells. (a-c) Subcutaneous tumor growth in immunodeficient NOG mice that received Pan02 cells stably expressing sh*ZDHHC9* or shControl Pan02 cells ($n = 6$ mice per group). Schematic of the treatment in tumor-bearing mice (a, $p = 0.0718$, t(2) = 2.013, df = 10). Representative images (b) and tumor weight (c, $p = 0.1076$, t(2) = 1.767, df = 10) of shControl and sh*ZDHHC9* tumors. (d, $p < 0.0001$, t(2) = 5.641, df = 14) Tumor inhibition rate for *ZDHHC9*^{KD} Pan02 cells and control cells after injection into C57BL/6 or immunodeficient NOG mice, respectively ($n = 10$ or 6 mice per group). (e-h) C57BL/6 mice were subcutaneously injected with shControl and sh*ZDHHC9* Pan02 cells and treated with CD8-depleting antibodies. Schematic of treatment (e), tumor growth curves (f; p(shControl+αCD8 vs sh*ZDHHC9*+αCD8) = 0.1815, q = 2.995; p(shControl+IgG vs sh*ZDHHC9*+ IgG)< 0.0001, q = 8.805), representative images (g), and tumor weight (h;; p(shControl+αCD8 vs sh*ZDHHC9*+αCD8) = 0.1139, q = 3.364; p(shControl+IgG vs sh*ZDHHC9*+ IgG)< 0.0001, q = 7.374) for tumor-bearing mice ($n = 6$ mice per group). (i-k) Representative flow cytometry dot plot of the CD8$^+$ T cell population in tumor and spleen samples obtained from shControl and sh*ZDHHC9* Pan02 tumor-bearing mice, injected with control isotype or CD8-depleting antibodies. Tumor and spleen tissues were isolated on day 21. CD8$^+$ T cells were defined as live CD45$^+$ CD8$^+$ cells and quantification ($n = 4$ mice per group). (l-n) C57BL/6 mice were subcutaneously injected with sh*ZDHHC9* Pan02 or LLC cells and received treatment with an anti-PD-L1 mAb or CD8a mAb ($n = 10$ mice per group). Schematic of treatment (l), tumor growth curves (m, $p = 0.0001$, t(2) = 4.899, df = 18), and tumor weight (n, $p = 0.0065$, t(2) = 3.077, df = 18) for tumor-bearing mice. (o-q) Representative flow cytometry dot plot of the CD8$^+$ T cell population in tumor (p, $p = 0.0012$, t(2) = 4.891, df = 8) and spleen (q, $p < 0.0001$, t(2) = 8.281, df = 8) samples obtained from Pan02 tumor-bearing mice injected with control isotype or CD8-depleting antibodies. CD8$^+$ T cells were defined as live CD45$^+$ CD8$^+$ cells and quantification (d) ($n = 7$ mice per group). (a, c, d, m, n, p, and q) p-values were calculated using a two-sided unpaired Student's t-test; (f, h, j, and k) p-values were calculated using a one-way ANOVA with a Tukey post hoc test. All results are presented as mean ± SD (ns = not significant, *$p < 0.05$, **$p < 0.01$, and ***$p < 0.001$).

cytometry (Fig. 5i-k). In mice inoculated with the shControl-treated Pan02 cells, treatment with the CD8α mAb treatment promoted tumor growth compared with the IgG2b control. Interestingly, the therapeutic effect of *ZDHHC9* KD was largely eliminated in animals treated with the anti-CD8 antibody (Fig. 5f-h). Thus, key members of the host immune system (e.g., CD8$^+$ T cells) are indispensable for the therapeutic effect of ZDHHC9 deficiency in tumor cells.

Accordingly, we reasoned that CD8$^+$ T cells are required for the synergistic effect exerted by the combination of ZDHHC9 deficiency and anti-PD-L1 therapy in pancreatic tumor models. We designed experiments to evaluate the anti-tumor efficacy of *ZDHHC9* KD plus anti-PD-L1 on CD8$^+$T cell-depleted immunocompetent mice. Notably, the efficient depletion of CD8$^+$ T cells in vivo (Fig. 5o-q) almost completely abolished the synergistic therapeutic effect of *ZDHHC9* KD and anti-PD-L1 on Pan02 tumors (Fig. 5l-n). These findings underscore the importance of CD8$^+$ T cells in pancreatic tumor regression following combination therapy. Furthermore, they suggest that tumor *ZDHHC9* KD effectively improves the immunosuppressive TME and sensitizes the tumor to anti-PD-L1 treatment in a CD8$^+$ T-cell-dependent manner.

3.7. Development of an NP-siZDHHC9-delivery system sensitized tumors to PD-L1 blockade in non-immunogenic models

The treatment effect of siRNA is often restricted by its susceptibility to degradation in vivo. To improve the translational potential of the RNA-based *ZDHHC9*-targeting strategy, we developed an advanced polymeric NP-based system for delivering *ZDHHC9*-siRNA to the tumor site. The NP-*ZDHHC9*-siRNA system (NP-si*ZDHHC9*) was composed of mPEG-PLGA and cationic lipids to protect the siRNA from degradation and effectively deliver *ZDHHC9* siRNA to the target cells. The construction of the siRNA delivery system is briefly illustrated in Fig. 6a. Following the construction of the NP-si*ZDHHC9*, the morphology of the resulting complex was initially characterized by TEM. As shown in Fig. 6b, the NP-si*ZDHHC9* assumed a typical spherical structure, which was consistent with the reported morphology of siRNA-loaded PEG-PLGA nanocomposites [58]. According to the TEM analysis, the average diameter of NP-si*ZDHHC9* was 146.5 ± 26.8 nm by TEM (Fig. 6c); this was also confirmed by dynamic light scattering (Fig. 6d). Additionally, the zeta potential of the nanocomposites was approximately + 47 mV (Fig. 6e), which was induced by the grafting of DOTAP. In addition, the NP-siRNA complexes showed high levels of biocompatibility in vitro. After co-culture with the NPs for 48 h, >90 % of the cells survived, even when the NP concentration reached 100 nM (Fig. S13a). Owing to the basic physiochemical properties of NPs (e.g., nanoscale diameter, amphipathic molecular structure, positive surface charge), NP-si*ZDHHC9* delivery was efficient and selective; however, it was not harmful to the target cells (Fig. 6f, g). The Pan02 cells were transfected with the NP-siRNA complexes to evaluate their gene silencing ability in

vitro. NP-si*ZDHHC9* resulted in 71.1 % gene silencing at the mRNA level compared with NP-si*NC* or naked si*NC* (Fig. 6h). Moreover, western blotting analysis revealed that the NP-si*ZDHHC9* group had lower levels of ZDHHC9 protein compared with the untreated (Mock) group. Furthermore, the silencing effect of NP-si*ZDHHC9* was maintained for 72 h after transfection, as confirmed by western blotting (Fig. 6i and Fig. S13b). The physiochemical properties, biocompatibility, delivery, and KD efficiency of the NPs confirmed the successful construction of an efficient si*ZDHHC9* delivery system.

Delivery systems focusing on maximizing the treatment outcome, while reducing systemic toxicity of co-delivered gene-silencing RNAs after local administration to tumors are often easily approved for clinical use [59]. Systemic drug delivery raises safety concerns, potentially leading to the use of suboptimal doses or even precluding the clinical development of such systems. Hence, intratumoral delivery is emerging as an attractive option for increasing the in-situ bioavailability and, thus, the efficacy of immunotherapies [60–62]. Accordingly, we further investigated the anti-tumor effect of *ZDHHC9* silencing via the intra-tumoral injection of NP-si*ZDHHC9* combined with PD-L1 blockade in the Pan02 and KPC tumor model. The reduction in ZDHHC9 expression of tumor tissues induced by NP-si*ZDHHC9* compared with the negative control NP-si*NC* was confirmed by RT-qPCR analysis (Fig. S13c, d). C57BL/6 mice were subcutaneously inoculated with Pan02 and KPC cells to evaluate the synergy between the two immunotherapeutic strategies. As expected, we observed that the anti-PD-L1 therapy was ineffective when used alone. While monotherapy with NP-si*ZDHHC9* reduced tumor growth, the combination of NP-si*ZDHHC9* and PD-L1 blockade markedly enhanced the efficacy and delayed Pan02 and KPC tumor progression (Fig. 6j-s). Four cycles of this combination treatment significantly prolonged survival time compared with saline-treated control (i.e., saline) (Fig. 6m, r). Importantly, the combination of NP-si*ZDHHC9* and anti-PD-L1 did not cause any mortality or induce significant reductions in body or spleen weight during treatment (Fig. S14a-c). Furthermore, there were no prominent inflammatory infiltrates or histological signs of toxicity in the main organs examined by H&E staining (Fig. S14d). Collectively, these data demonstrate that treatment with NP-si*ZDHHC9* restored tumor sensitivity to anti-PD-L1, thus offering a promising therapeutic strategy for refractory Pan02 and KPC tumor models.

3.8. Combination therapy with the NP-siZDHHC9-delivery system and PD-L1 blockade expands CD8$^+$ T cells and lowers CD11b$^+$Gr-1$^+$MDSC numbers in tumors

We sought to further determine the effect of PD-L1 pathway blockade in combination with ZDHHC9 KD on the immune cell composition of tumors. Therfore, we isolated the tumor-infiltrating leukocytes and conducted flow cytometry analysis. Notably, we observed that the

strong synergistic therapeutic effect was associated with a marked increase in the frequency of CD8^{+} T cell infiltration in the tumor. This was accompanied by a reduction in the populations of PD-1^{+} CD8^{+} T cells and CD11b^{+}Gr-1^{+} MDSCs in KPC tumors (Fig. 7a-c). In Pan02 tumors, the numbers of CD8^{+} T cells and CD4^{+} T cells were 5.7-fold and 3.2-fold greater, respectively, in the NP-si*ZDHHC9* +anti-PD-L1 group than in the vehicle group (Fig. S15a, b). ZDHHC9 KD in KPC tumors increased the infiltration of CD8^{+} T cells and enhanced GZMB production, as confirmed by the IHC staining of tumor sections (Fig. 7d, e). Moreover, ZDHHC9 deficiency boosted the population of tumor-infiltrating CD8^{+} T

cells, as well as the production of GZMB, TNF-α, IFN-γ, and IL-12p70; these effects were indicative of cytotoxic T cell-mediated adaptive immunity (Fig. 7d, e and Fig. S16a). The combined ZDHHC9 and PD-L1 inhibition increased the infiltration and activity of CD8^{+} T cells, and reversed the immunosuppressives state of the TME, as evidenced by a decrease in IL-10 secretion and Gr-1 expression (Fig. S16b). These results suggest that ZDHHC9 deficient and PD-L1 blockade induce a reduction in the number of MDSC. These effects may lead to the abolishment of immune inhibition, as well as promote the infiltration of T cells in into the pancreatic tumor and their subsequent activation.
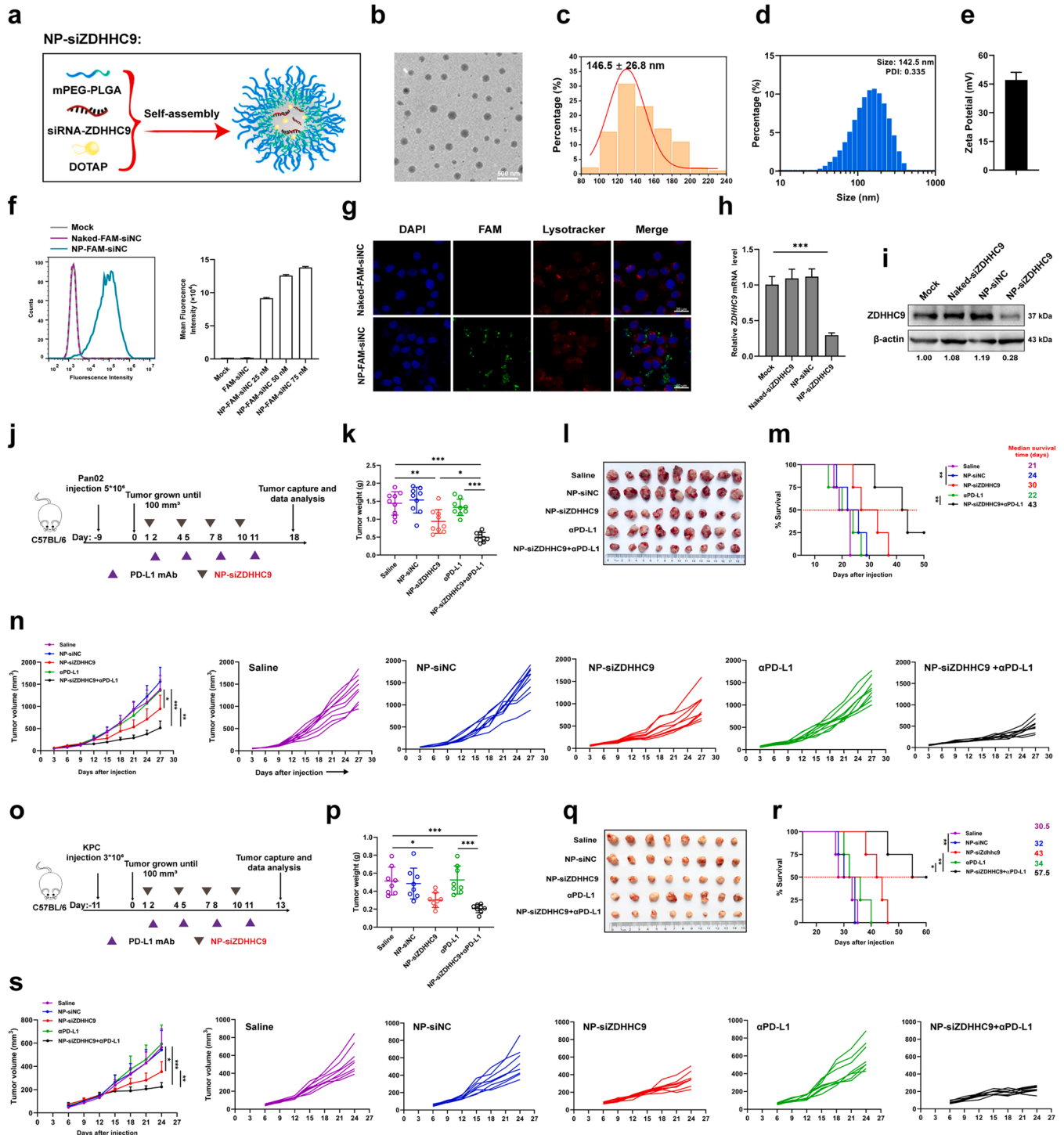
(caption on next page)

Fig. 6. The combination of NP-siZDHHC9 and anti-PD-L1 immunotherapy delayed tumor growth and showed the therapeutic potential in the Pan02 and KPC tumor model. (a) Process for the preparationof NP-si*ZDHHC9*. (b-e) Biophysical characterization of siRNA nanomedicines. The morphology (b) and hydrodynamic diameter (c) of NP-siRNA were characterized by TEM. Size distribution (d) and zeta potential (e) of the NP-siRNA complexes. (f) The cellular uptake efficiency of the NP-siRNA complexes was analyzed by flow cytometry to evaluate the efficiency of in vitro internalization. The mean fluorescence intensity (MFI) was recorded using the assay measuring the cellular uptake of siRNA nanomedicines. (g) Transfection of Pan02 cells with NP-FAM-siRNA complexes was confirmed by confocal laser scanning microscopy (CLSM); scale bar = 20 μm. (h, p(Mock vs NP-si*ZDHHC9*) = 0.0001, q = 12.04) The relative efficiency of *ZDHHC9* mRNA KD was determined by RT-PCR. (i) The relative efficiency of ZDHHC9 protein KD was determined by immunoblotting assay. (j-s) Scheme of the treatment plan (j). Mice with Pan02 and KPC tumors were intratumorally injected with siRNA nanomedicines. Tumor weights (k, p), representative tumor images (l, q), and mice survival curves (m, r) were recorded at the end of the experiment. Tumor weight (k): p(saline vs NP-si*ZDHHC9*+αPD-L1) < 0.0001, q= 9.823; p(NP-si*ZDHHC9* vs NP-si*ZDHHC9*+αPD-L1) = 0.0197, q = 4.569; p(αPD-L1 vs NP-si*ZDHHC9*+αPD-L1) < 0.0001, q = 8.651); Survival (m): p(saline vs NP-si*ZDHHC9*) = 0.0091, Chi square = 6.8; p(αPD-L1 vs NP-si*ZDHHC9*+αPD-L1) = 0.0067, Chi square = 7.344); Tumor volume (n): p(saline vs NP-si*ZDHHC9*+αPD-L1) < 0.0001, q = 9.451; p(saline vs NP-si*ZDHHC9*) = 0.014, q = 4.756; p(αPD-L1 vs NP-si*ZDHHC9*+αPD-L1) < 0.0001, q = 9.137). Tumor weight (p): p(saline vs NP-si*ZDHHC9*+αPD-L1) = 0.0004, q = 6.594; p(NP-si*ZDHHC9* vs NP-si*ZDHHC9*+αPD-L1) = 0.0219, q = 4.549; p(αPD-L1 vs NP-si*ZDHHC9*+αPD-L1) = 0.0002, q = 6.837); Survival (r): p(saline vs NP-si*ZDHHC9*) = 0.0067, Chi square = 7.344; p(αPD-L1 vs NP-si*ZDHHC9*+αPD-L1) = 0.0114, Chi square = 6.4); Tumor volume (s): p(saline vs NP-si*ZDHHC9*+αPD-L1) = 0.0001, q = 7.257; p (saline vs NP-si*ZDHHC9*) = 0.0256, q = 4.46; p(αPD-L1 vs NP-si*ZDHHC9*+αPD-L1) < 0.0001, q = 7.899).The average and individual tumor growth curves for mice subcutaneously injected with Pan02 (n) or KPC (s) parental tumors after different treatments (n = 9 or 8 mice per group). All results are presented as mean ± SD. (h, k, n, p, and s) p-values were calculated using a one-way ANOVA with a Tukey post hoc test. Survival curves for the groups were analyzed using the log-rank (Mantel-Cox) test (*p < 0.05, **p < 0.01, and ***p < 0.001).

3.9. Reduced ZDHHC9 and PD-L1 expression improved the prognosis of untreated patients with PAAD

Based on the above results, we questioned whether the reduced expression *ZDHHC9* and *PD-L1* within the TME of patients with PAAD was associated with a more favourable prognosis. Therefore, we assessed the correlation between the mRNA expression levels of *ZDHHC9* and *PD-L1* in cells in the TME and survival time of patients with PAAD using data from the TCGA database. We initially found that PAAD patients with low *ZDHHC9* expression lived longer than those with high *ZDHHC9* expression, with the median survival time improving from 20.23 months to 31.57 months (Fig. S17a). However, there was no significant difference in survival time between patients with high or low *PD-L1* expression (Fig. S17b). Notably, the subpopulation of PAAD patients with low *ZDHHC9* and *PD-L1* expression had a median survival time of 72.73 months. This was significantly longer than the median survival time of 17.73 months for patients with high *ZDHHC9* expression and low *PD-L1* expression (Fig. S17c). Similarly, in the subpopulation of patients with low *ZDHHC9* expression, the median survival was improved from 23.9 months to 72.53 months in patients with low *PD-L1* expression versus those with high *PD-L1* expression; however, there was no significant improvement in median-free survival (Fig. S17d). Overall, these findings indicate that *ZDHHC9*^{KD} may synergize with anti-PD-L1 immunotherapy in human pancreatic cancer.

4. Discussion

Protein lipidation is a prototypical form of post-translational modification, in which S-palmitoylation exerts multiple effects to dynamically orchestrate the interactions and functions of target protein. The majority of S-palmitoylated proteins are catalyzed by a family of ZDHHC enzymes. Recent studies have shown that *ZDHHC9* knockout attenuated the progression of T-cell acute lymphoblastic leukemia and chronic granulocytic leukemia driven by the *NRAS*^{G12D} mutation. Furthermore, *ZDHHC9* knockout in tumor cells suppressed tumor progression of glioblastoma by inhibiting palmitoylation of glucose transporter type 1 (GLUT1) and, consequently, tumor cell proliferation [30]. In addition, ZDHHC9 is also differentially expressed in patients with microsatellite-stable and unstable colorectal cancer [63]. It has been shown that enhancement of enhancing ZDHHC9-mediated palmitoylation was able to stabilize the protein levels of PD-L1 and PD-1 in tumor cells [36,64]. In the present study, we investigated the mRNA expression of ZDHHC9 in human cancer tissues and its protein expression in clinical pancreatic cancer samples. We found that ZDHHC9 was significantly upregulated in pancreatic cancer tissues compared with normal tissues and was associated with poor prognosis. Moreover, we found that ZDHHC9 deficiency in pancreatic cancer cells inhibited tumor growth

and prolonged the survival of mice by enhancing anti-tumor immunity.

ICB therapy is significantly hampered by a highly immunosuppressive TME and a lack of pre-existing immune cell infiltration within the pancreatic tumor, indicating that numerous patients with pancreatic cancer fail to respond to this novel form of ICB treatment [10]. The expression of inhibitory immune checkpoint proteins, such as PD-L1, is elevated following the reversal of the 'cold' TME state, due to the regulation of negative feedback. In this study, using pancreatic tumor tissues, we demonstrated that ZDHHC9 deficiency increased the expression of PD-L1 in multiple immune cells and enhanced the number and function of tumor-infiltrated activated T-cells. Our results support the role of ZDHHC9 as a key molecular switch protein influencing the tumor immune microenvironment. In addition, these results emphasize the need to exploit the therapeutic potential of ZDHHC9 in pancreatic tumor cells for boosting the potency of anti-PD-1/PD-L1 therapy. We have demonstrated that the KD or inhibition of ZDHHC9 can drastically increase the efficiency of anti-PD-L1 treatment in ICB-refractory Pan02 and KPC tumors. Further support for this strategy is provided by the robust and synergistic effects of the combination treatment with NP-si*ZDHHC9* and anti-PD-L1, as demonstrated in the poorly immunogenic Pan02 and KPC tumors. ZDHHC9 inhibition by si*ZDHHC9*-loaded NPs restored tumor sensitivity to anti-PD-L1, suppressed pancreatic tumor growth, and markedly prolonged the survival time of mice. Therefore, ZDHHC9 may represent a novel therapeutic target and diagnostic biomarker for pancreatic cancer. Further detailed analysis should be conducted to determine the value of ZDHHC9 inactivation in the development of novel treatments for patients with pancreatic cancer, including those with metastatic, locally advanced, borderline resectable, and surgically resected tumors. More importantly, future studies should further evaluate the clinical utility of this approach, including the potential ability of ZDHHC9 to predict and monitor the clinical benefit of immunotherapy in patients with PAAD. The predictive value of ZDHHC9 expression (that changes after better clinical recovery) for disease relapses and the need of chronic immunotherapy interventions should also be investigated.

The pro-inflammatory TME is also characterized by the upregulation of inhibitory immune checkpoint proteins (e.g., PD-L1/PD-1), which is driven by pre-infiltrating CD8$^+$ T cells [65]. These immune checkpoint molecules suppress pre-existing cancer immunity to avoid an overactive immune response and result in immune evasion. In our study, the increased PD-L1 expression in CD11b$^+$ myeloid cells, F4/80$^+$ macrophages, and DCs might be attributed to the enhanced infiltration of intra-tumoral CD8$^+$ T cells in *ZDHHC9*^{KD} Pan02 tumors. The elevated expression of ZDHHC9 in tumor cells attenuated CD8$^+$-T-cell-mediated cytotoxicity in tumor cells by enhancing the membrane distribution and stability of PD-L1. These findings are consistent with those of recent studies reporting that the localization and stability of the key immune
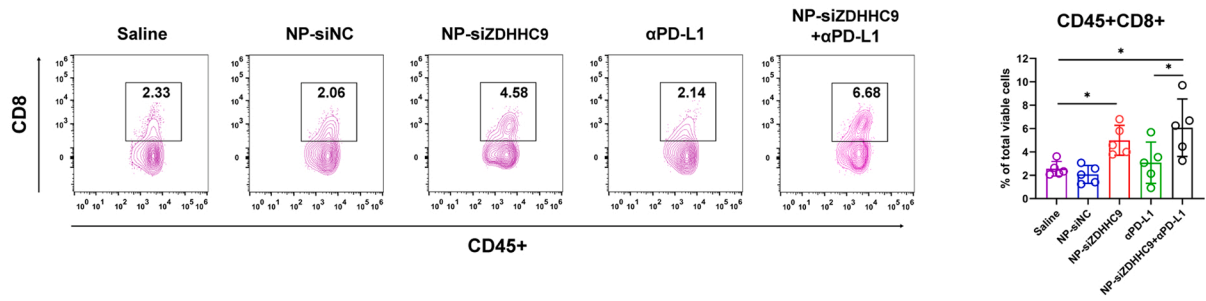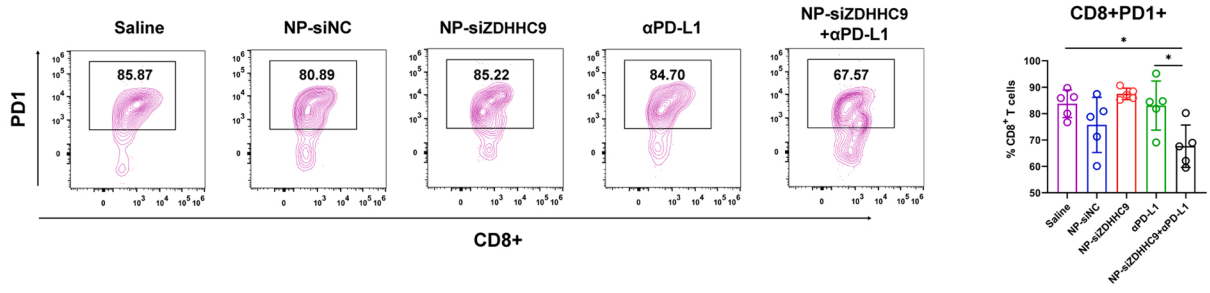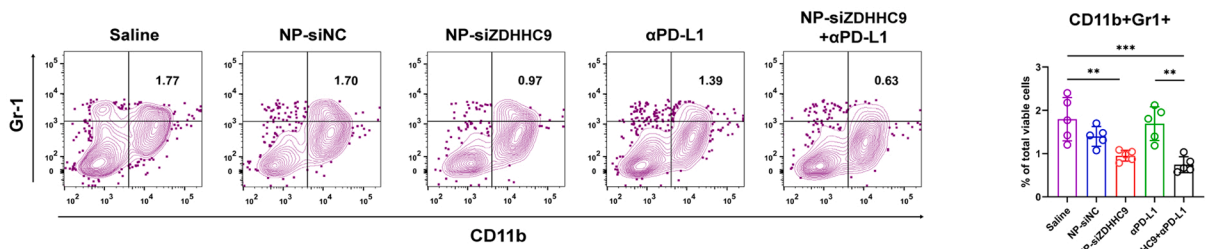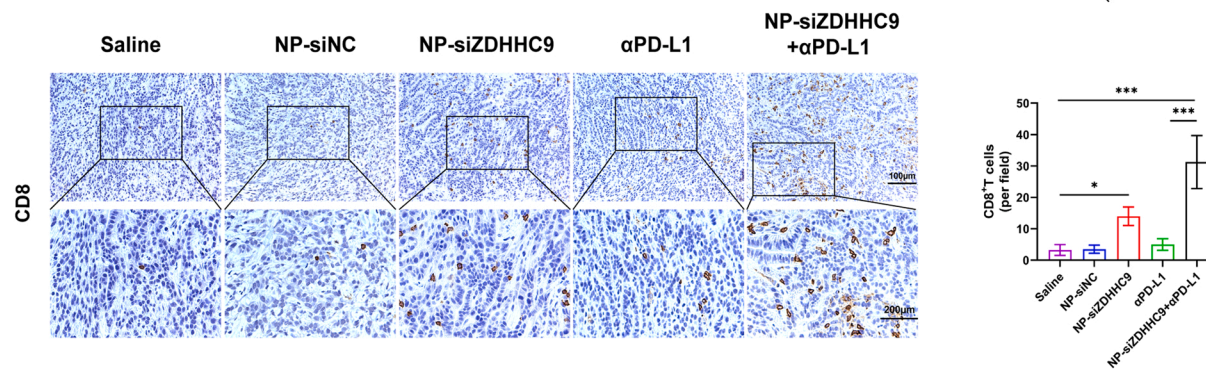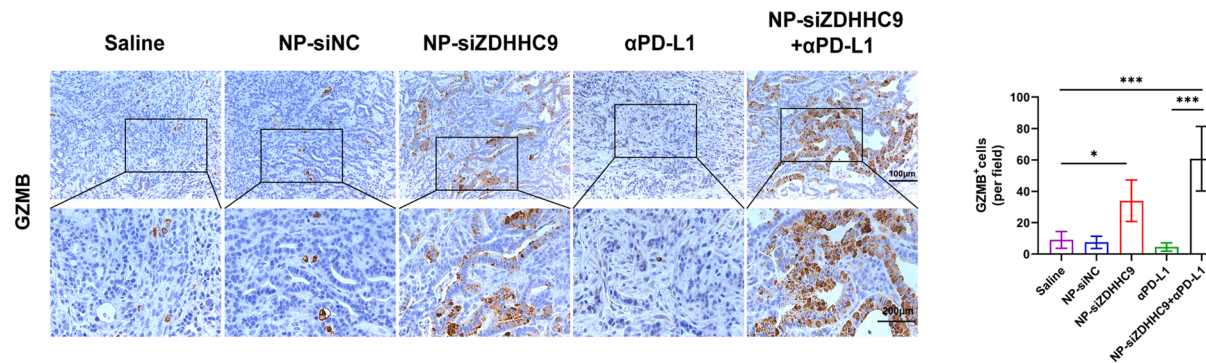
(caption on next page)

Fig. 7. The combination therapy comprising ZDHHC9 deficiency and PD-L1 blockade augmented tumor infiltration by T cells. KPC tumor-bearing mice were euthanized and tumor tissues were isolated after the fourth cycle of treatment. (a-c) Representative flow cytometric analyses and quantitation of tumor-infiltrating immune cells in KPC tumors including $CD45^+$ $CD8^+$ T cells (a, p(saline vs NP-si*ZDHHC9*+αPD-L1) = 0.0133, q = 5.109; p(saline vs NP-si*ZDHHC9*) = 0.0485, q = 4.253; p(αPD-L1 vs NP-si*ZDHHC9*+αPD-L1) = 0.0413, q = 4.363), $PD-1^+$ $CD8^+$ T cells (b, p(saline vs NP-si*ZDHHC9*+αPD-L1) = 0.0252, q = 4.695; p(αPD-L1 vs NP-si*ZDHHC9*+αPD-L1) = 0.034, q = 4.495), and $CD11b^+$ $Gr1^+$ myeloid cells (c, p(saline vs NP-si*ZDHHC9*+αPD-L1) = 0.0004, q = 7.384; p(saline vs NP-si*ZDHHC9*) = 0.0036, q = 5.934; p(αPD-L1 vs NP-si*ZDHHC9*+αPD-L1) = 0.0011, q = 6.658) on day 24 after KPC tumor inoculation and quantification (n = 5 mice per group). All results are presented as mean ± SD. (d and e) Representative images of IHC staining for CD8 (d) and GZMB (e) of tumor tissues extracted from mice at the end of the experiment and the corresponding quantification (CD8: p(saline vs NP-si*ZDHHC9*+αPD-L1) < 0.0001, q = 13.34; p(saline vs NP-si*ZDHHC9*) = 0.0182, q = 5.120; p(αPD-L1 vs NP-si*ZDHHC9*+αPD-L1) < 0.0001, q = 12.50); (GZMB: p(saline vs NP-si*ZDHHC9*+αPD-L1) < 0.0001, q = 9.080; p(saline vs NP-si*ZDHHC9*) = 0.0487, q = 4.387; p(αPD-L1 vs NP-si*ZDHHC9*+αPD-L1) < 0.0001, q = 9.870)scale bars = 100 μm. (a-e) p-values were calculated using a one-way ANOVA with a Tukey post hoc test (*p < 0.05, **p < 0.01, and ***p < 0.001).

checkpoint proteins PD-1 and PD-L1 in tumor cells are regulated by ZDHHC9-mediated palmitoylation [28,36].

Thus far, there are no potent and specific inhibitors of ZDHHC. Large drug-screening programs targeting the ZDHHC family have identified 2-bromopalmitate, a broad-spectrum palmitoylation inhibitor. 2-bromo-palmitate has been used in the preclinical validation of the involvement of ZDHHC protein in cancer growth. However, its non-selective targeting and off-target acylation of other intracellular proteins render it an undesirable drug candidate. In addition, each specific protein belonging to the ZDHHC family has distinct biological functions (e.g., regulation of neuropsychiatric behavior) and roles in tumor pathogenesis. The lack of specific inhibitors of ZDHHC9 hinders the translational potential of this protein as a therapeutic target. Recently, the use of gene-silencing siRNAs has been explored as a promising option for the treatment of cancer treatment [66–68]. Several siRNA-based drugs (e.g., patisiran and givosiran) have been successfully developed and received approval by the US Food and Drug Administration or have entered an advanced stage of clinical trials for the treatment of renal disease and dry eye syndrome [69,70]. However, numerous critical challenges should be addressed before siRNAs can be routinely used in clinical practice, such as their unsatisfactory stability, poor cellular uptake, and off-target effects [71]. We selected polymer NPs as a promising drug delivery system to deliver si*ZDHHC9* to tumors [48,59,67,72,73]. NPs have notable biophysical and pharmacological features, such as higher tissue permeability, high stability and biocompatibility, and tumor-targeting properties.

5. Conclusions

In this study, we developed a polymeric NP approach for the in vivo delivery of si*ZDHHC9* to tumor tissues to test the efficacy of combined si*ZDHHC9* and PD-L1 immunotherapy. The NP-si*ZDHHC9* delivery system exhibited excellent siRNA stability, biocompatibility, and ZDHHC9 silencing in pancreatic tumor cells. Importantly, the direct intra-tumoral administration of NPs packaged with si*ZDHHC9* successfully triggered anti-tumor immune responses by inducing the recruitment of activated $CD8^+$ T cells and enhancing the expression of pro-inflammatory cytokines. Further studies are warranted to optimize the dosage and delivery of NP-si*ZDHHC9*, or explore other methods for selectively and accurately delivering si*ZDHHC9* to the pancreatic tumor site. In summary, the present findings demonstrated that the inactivation of ZDHHC9 may be an effective immunotherapeutic strategy and booster for anti-PD-L1 therapy in pancreatic cancer, with promising implications for other forms of ICB.

CRediT authorship contribution statement

Zhiqing Lin, Keke Huang : Conceptualization, Methodology, Investigation, Writing of the original draft. **Hui Guo:** Methodology, Investigation. **Manli Jia:** Methodology (Bioinformatics). **Qiuqin Sun, Xuhao Chen:** Investigation, Draft reviewing and editing. **Qingqing Yao, Peng Zhang, Sergii Vakal, Zhengzhi Zou, Haiyao Gao, Lei Ci:** Resources. **Jiangfan Chen:** Data curation, Funding acquisition, Supervision, Draft reviewing and editing. **Wei Guo:** Conceptualization, Data

curation, Funding acquisition, Writing of the original draft, Draft reviewing and editing.

Conflict of Interest Statement

The authors declare that they have no known competing financial interests or personal relationships that could have appeared to influence the work reported in this paper.

Data Availability

Data will be made available on request.

Appendix A. Supporting information

Supplementary data associated with this article can be found in the online version at doi:10.1016/j.biopha.2023.114567.

References

[1] D. Schizas, N. Charalampakis, C. Kole, P. Economopoulou, E. Koustas, E. Gkotsis, D. Ziogas, A. Psyrri, M.V. Karamouzis, Immunotherapy for pancreatic cancer: a 2020 update, Cancer Treat. Rev. 86 (2020), 102016.

[2] S. Abe, H. Nagata, E.J. Crosby, Y. Inoue, K. Kaneko, C.X. Liu, X. Yang, T. Wang, C. R. Acharya, P. Agarwal, J. Snyder, W. Gwin, M.A. Morse, P. Zhong, H.K. Lyerly, T. Osada, Combination of ultrasound-based mechanical disruption of tumor with immune checkpoint blockade modifies tumor microenvironment and augments systemic antitumor immunity, J. Immunother. Cancer 10 (2022).

[3] A. Di Federico, V. Tateo, C. Parisi, F. Formica, R. Carloni, G. Frega, A. Rizzo, D. Ricci, M. Di Marco, A. Palloni, G. Brandi, Hacking pancreatic cancer: present and future of personalized medicine, Pharmaceuticals (Basel) 14 (2021).

[4] D.D. Von Hoff, T. Ervin, F.P. Arena, E.G. Chiorean, J. Infante, M. Moore, T. Seay, S. A. Tjulandin, W.W. Ma, M.N. Saleh, M. Harris, M. Reni, S. Dowden, D. Laheru, N. Bahary, R.K. Ramanathan, J. Tabernero, M. Hidalgo, D. Goldstein, E. Van Cutsem, X. Wei, J. Iglesias, M.F. Renschler, Increased survival in pancreatic cancer with nab-paclitaxel plus gemcitabine, N. Engl. J. Med. 369 (2013) 1691–1703.

[5] R. De Luca, L. Gianotti, P. Pedrazzoli, O. Brunetti, A. Rizzo, M. Sandini, S. Paiella, N. Pecorelli, L. Pugliese, A. Pietrabissa, R. Zerbi, R. Salvia, U. Boggi, A. Casirati, M. Falconi, R. Caccialanza, Immunonutrition and prehabilitation in pancreatic cancer surgery: a new concept in the era of ERAS® and neoadjuvant treatment, Eur. J. Surg. Oncol. 49 (2023) 542–549.

[6] V.P. Balachandran, G.L. Beatty, S.K. Dougan, Broadening the impact of immunotherapy to pancreatic cancer: challenges and opportunities, Gastroenterology 156 (2019) 2056–2072.

[7] G. Viscardi, A.C. Tralongo, F. Massari, M. Lambertini, V. Mollica, A. Rizzo, F. Comito, R. Di Liello, S. Alfieri, M. Imbimbo, C.M. Della Corte, F. Morgillo, V. Simeon, G. Lo Russo, C. Proto, A. Prelaj, A. De Toma, G. Galli, D. Signorelli, F. Ciardiello, J. Remon, N. Chaput, B. Besse, F. de Braud, M.C. Garassino, V. Torri, M. Cinquini, R. Ferrara, Comparative assessment of early mortality risk upon immune checkpoint inhibitors alone or in combination with other agents across solid malignancies: a systematic review and meta-analysis, Eur. J. Cancer 177 (2022) 175–185.

[8] H. Borghaei, L. Paz-Ares, L. Horn, D.R. Spigel, M. Steins, N.E. Ready, L.Q. Chow, E. E. Vokes, E. Felip, E. Holgado, F. Barlesi, M. Kohlhaufl, O. Arrieta, M.A. Burgio, J. Fayette, H. Lena, E. Poddubskaya, D.E. Gerber, S.N. Gettinger, C.M. Rudin, N. Rizvi, L. Crino, G.R. Blumenschein Jr., S.J. Antonia, C. Dorange, C.T. Harbison, F. Graf Finckenstein, J.R. Brahmer, Nivolumab versus docetaxel in advanced nonsquamous non-small-cell lung cancer, N. Engl. J. Med. 373 (2015) 1627–1639.

[9] J.R. Brahmer, S.S. Tykodi, L.Q. Chow, W.J. Hwu, S.L. Topalian, P. Hwu, C. G. Drake, L.H. Camacho, J. Kauh, K. Odunsi, H.C. Pitot, O. Hamid, S. Bhatia, R. Martins, K. Eaton, S. Chen, T.M. Salay, S. Alaparthy, J.F. Grosso, A.J. Korman, S. M. Parker, S. Agrawal, S.M. Goldberg, D.M. Pardoll, A. Gupta, J.M. Wigginton, Safety and activity of anti–PD-L1 antibody in patients with advanced cancer, N. Engl. J. Med. 366 (2012) 2455–2465.

[10] J. Galon, D. Bruni, Approaches to treat immune hot, altered and cold tumours with combination immunotherapies, Nat. Rev. Drug Disco 18 (2019) 197–218.

[11] M. Sznol, L. Chen, Antagonist antibodies to PD-1 and B7-H1 (PD-L1) in the treatment of advanced human cancer–response, Clin. Cancer Res 19 (2013) 5542.

[12] A.S. Bear, R.H. Vonderheide, M.H. O'Hara, Challenges and opportunities for pancreatic cancer immunotherapy, Cancer Cell 38 (2020) 788–802.

[13] P. Sharma, S. Hu-Lieskovan, J.A. Wargo, A. Ribas, Primary, adaptive, and acquired resistance to cancer immunotherapy, Cell 168 (2017) 707–723.

[14] M.F. Sanmamed, L. Chen, A paradigm shift in cancer immunotherapy: from enhancement to normalization, Cell 175 (2018) 313–326.

[15] S.P. Kubli, T. Berger, D.V. Araujo, L.L. Siu, T.W. Mak, Beyond immune checkpoint blockade: emerging immunological strategies, Nat. Rev. Drug Disco 20 (2021) 899–919.

[16] Y. Pylayeva-Gupta, K.E. Lee, C.H. Hajdu, G. Miller, D. Bar-Sagi, Oncogenic Kras-induced GM-CSF production promotes the development of pancreatic neoplasia, Cancer Cell 21 (2012) 836–847.

[17] S.R. Hingorani, L. Wang, A.S. Multani, C. Combs, T.B. Deramaudt, R.H. Hruban, A. K. Rustgi, S. Chang, D.A. Tuveson, Trp53R172H and KrasG12D cooperate to promote chromosomal instability and widely metastatic pancreatic ductal adenocarcinoma in mice, Cancer Cell 7 (2005) 469–483.

[18] J. Galon, A. Costes, F. Sanchez-Cabo, A. Kirilovsky, B. Mlecnik, C. Lagorce-Pages, M. Tosolini, M. Camus, A. Berger, P. Wind, F. Zinzindohoue, P. Bruneval, P. H. Cugnenc, Z. Trajanoski, W.H. Fridman, F. Pages, Type, density, and location of immune cells within human colorectal tumors predict clinical outcome, Science 313 (2006) 1960–1964.

[19] H. Angell, J. Galon, From the immune contexture to the immunoscore: the role of prognostic and predictive immune markers in cancer, Curr. Opin. Immunol. 25 (2013) 261–267.

[20] W.C. Cheng, Y.C. Tsui, S. Ragusa, V.H. Koelzer, M. Mina, F. Franco, H. Laubli, B. Tschumi, D. Speiser, P. Romero, A. Zippelius, T.V. Petrova, K. Mertz, G. Ciriello, P.C. Ho, Uncoupling protein 2 reprograms the tumor microenvironment to support the anti-tumor immune cycle, Nat. Immunol. 20 (2019) 206–217.

[21] S. Bhatia, A. Oweida, S. Lennon, L.B. Darragh, D. Milner, A.V. Phan, A.C. Mueller, B. Van Court, D. Raben, N.J. Serkova, X.J. Wang, A. Jimeno, E.T. Clambey, E. B. Pasquale, S.D. Karam, Inhibition of EphB4-Ephrin-B2 signaling reprograms the tumor immune microenvironment in head and neck cancers, Cancer Res. 79 (2019) 2722–2735.

[22] K. Lemonidis, M.W. Werno, J. Greaves, C. Diez-Ardanuy, M.C. Sanchez-Perez, C. Salaun, D.M. Thomson, L.H. Chamberlain, The zDHHC family of S-acyltransferases, Biochem Soc. Trans. 43 (2015) 217–221.

[23] M.E. Linder, R.J. Deschenes, Palmitoylation: policing protein stability and traffic, Nat. Rev. Mol. Cell Biol. 8 (2007) 74–84.

[24] L.H. Chamberlain, M.J. Shipston, The physiology of protein S-acylation, Physiol. Rev. 95 (2015) 341–376.

[25] P.J. Ko, S.J. Dixon, Protein palmitoylation and cancer, EMBO Rep. 19 (2018) e46666.

[26] X. Chen, H. Ma, Z. Wang, S. Zhang, H. Yang, Z. Fang, EZH2 palmitoylation mediated by ZDHHC5 in p53-mutant glioma drives malignant development and progression, Cancer Res. 77 (2017) 4998–5010.

[27] C. Sharma, H.X. Wang, Q. Li, K. Knoblich, E.S. Reisenbichler, A.L. Richardson, M. E. Hemler, Protein acyltransferase DHHC3 regulates breast tumor growth, oxidative stress, and senescence, Cancer Res. 77 (2017) 6880–6890.

[28] H. Yao, J. Lan, C. Li, H. Shi, J.P. Brosseau, H. Wang, H. Lu, C. Fang, Y. Zhang, L. Liang, X. Zhou, C. Wang, Y. Xue, Y. Cui, J. Xu, Inhibiting PD-L1 palmitoylation enhances T-cell immune responses against tumours, Nat. Biomed. Eng. 3 (2019) 306–317.

[29] X. Chen, A. Hao, X. Li, K. Ye, C. Zhao, H. Yang, H. Ma, L. Hu, Z. Zhao, L. Hu, F. Ye, Q. Sun, H. Zhang, H. Wang, X. Yao, Z. Fang, Activation of JNK and p38 MAPK mediated by ZDHHC17 rives glioblastoma multiforme development and malignant progression, Theranostics 10 (2020) 998–1015.

[30] Z. Zhang, X. Li, F. Yang, C. Chen, P. Liu, Y. Ren, P. Sun, Z. Wang, Y. You, Y.X. Zeng, X. Li, DHHC9-mediated GLUT1 S-palmitoylation promotes glioblastoma glycolysis and tumorigenesis, Nat. Commun. 12 (2021) 5872.

[31] P. Liu, B. Jiao, R. Zhang, H. Zhao, C. Zhang, M. Wu, D. Li, X. Zhao, Q. Qiu, J. Li, R. Ren, Palmitoylacyltransferase Zdhhc9 inactivation mitigates leukemogenic potential of oncogenic Nras, Leukemia 30 (2016) 1225–1228.

[32] M. Yuan, X. Chen, Y. Sun, L. Jiang, Z. Xia, K. Ye, H. Jiang, B. Yang, M. Ying, J. Cao, Q. He, ZDHHC12-mediated claudin-3 S-palmitoylation determines ovarian cancer progression, Acta Pharm. Sin. B 10 (2020) 1426–1439.

[33] S. Chen, C. Han, X. Miao, X. Li, C. Yin, J. Zou, M. Liu, S. Li, L. Stawski, B. Zhu, Q. Shi, Z.X. Xu, C. Li, C.R. Goding, J. Zhou, R. Cui, Targeting MC1R depalmitoylation to prevent melanomagenesis in redheads, Nat. Commun. 10 (2019) 877.

[34] S. Chen, B. Zhu, C. Yin, W. Liu, C. Han, B. Chen, T. Liu, X. Li, X. Chen, C. Li, L. Hu, J. Zhou, Z.X. Xu, X. Gao, X. Wu, C.R. Goding, R. Cui, Palmitoylation-dependent activation of MC1R prevents melanomagenesis, Nature 549 (2017) 399–403.

[35] J.T. Swarthout, S. Lobo, L. Farh, M.R. Croke, W.K. Greentree, R.J. Deschenes, M. E. Linder, DHHC9 and GCP16 constitute a human protein fatty acyltransferase with specificity for H- and N-Ras, J. Biol. Chem. 280 (2005) 31141–31148.

[36] H. Yao, C. Li, F. He, T. Song, J.P. Brosseau, H. Wang, H. Lu, C. Fang, H. Shi, J. Lan, J.Y. Fang, J. Xu, A peptidic inhibitor for PD-1 palmitoylation targets its expression and functions, RSC Chem. Biol. 2 (2021) 192–205.

[37] M. Ayers, J. Lunceford, M. Nebozhyn, E. Murphy, A. Loboda, D.R. Kaufman, A. Albright, J.D. Cheng, S.P. Kang, V. Shankaran, S.A. Piha-Paul, J. Yearley, T. Y. Seiwert, A. Ribas, T.K. McClanahan, IFN-gamma-related mRNA profile predicts clinical response to PD-1 blockade, J. Clin. Invest 127 (2017) 2930–2940.

[38] H. Liu, X. Kuang, Y. Zhang, Y. Ye, J. Li, L. Liang, Z. Xie, L. Weng, J. Guo, H. Li, F. Ma, X. Chen, S. Zhao, J. Su, N. Yang, F. Fang, Y. Xie, J. Tao, J. Zhang, M. Chen, C. Peng, L. Sun, X. Zhang, J. Liu, L. Han, X. Xu, M.C. Hung, X. Chen, ADORA1 inhibition promotes tumor immune evasion by regulating the ATF3-PD-L1 axis, Cancer Cell 37 (2020) 324–339, e328.

[39] K. Huang, X. Liu, Z. Lv, D. Zhang, Y. Zhou, Z. Lin, J. Guo, MMP9-responsive graphene oxide quantum dot-based nano-in-micro drug delivery system for combinatorial therapy of choroidal neovascularization, Small (2023), e2207335.

[40] H. Jiang, S. Hegde, B.L. Knolhoff, Y. Zhu, J.M. Herndon, M.A. Meyer, T. M. Nywening, W.G. Hawkins, I.M. Shapiro, D.T. Weaver, J.A. Pachter, A. Wang-Gillam, D.G. DeNardo, Targeting focal adhesion kinase renders pancreatic cancers responsive to checkpoint immunotherapy, Nat. Med. 22 (2016) 851–860.

[41] M.Z. Noman, S. Parpal, K. Van Moer, M. Xiao, Y. Yu, J. Viklund, A. De Milito, M. Hasmim, M. Andersson, R.K. Amaravadi, J. Martinsson, G. Berchem, B. Janji, Inhibition of Vps34 reprograms cold into hot inflamed tumors and improves anti–PD-1/PD-L1 immunotherapy, Sci. Adv. 6 (2020) eaax7881.

[42] K. Huang, Z. Lin, Y. Ge, X. Chen, Y. Pan, Z. Lv, X. Sun, H. Yu, J. Chen, Q. Yao, Immunomodulation of MiRNA-223-based nanoplatform for targeted therapy in retinopathy of prematurity, J. Control Release 350 (2022) 789–802.

[43] L. Chen, F. Rashid, A. Shah, H.M. Awan, M. Wu, A. Liu, J. Wang, T. Zhu, Z. Luo, G. Shan, The isolation of an RNA aptamer targeting to p53 protein with single amino acid mutation, Proc. Natl. Acad. Sci. U. S. A. 112 (2015) 10002–10007.

[44] C. Li, Z. Tang, W. Zhang, Z. Ye, F. Liu, GEPIA2021: integrating multiple deconvolution-based analysis into GEPIA, Nucleic Acids Res. 49 (2021) W242–W246.

[45] M.S. Rooney, S.A. Shukla, C.J. Wu, G. Getz, N. Hacohen, Molecular and genetic properties of tumors associated with local immune cytolytic activity, Cell 160 (2015) 48–61.

[46] B. Ru, C.N. Wong, Y. Tong, J.Y. Zhong, S.S.W. Zhong, W.C. Wu, K.C. Chu, C. Y. Wong, C.Y. Lau, I. Chen, N.W. Chan, J. Zhang, TISIDB: an integrated repository portal for tumor-immune system interactions, Bioinformatics 35 (2019) 4200–4202.

[47] Y.T. Liu, Z.J. Sun, Turning cold tumors into hot tumors by improving T-cell infiltration, Theranostics 11 (2021) 5365–5386.

[48] Q.Q. Duan, H.L. Zhang, J.N. Zheng, L.J. Zhang, Turning cold into hot: firing up the tumor microenvironment, Trends Cancer 6 (2020) 605–618.

[49] P. Charoentong, F. Finotello, M. Angelova, C. Mayer, M. Efremova, D. Rieder, H. Hackl, Z. Trajanoski, Pan-cancer immunogenomic analyses reveal genotype-immunophenotype relationships and predictors of response to checkpoint blockade, Cell Rep. 18 (2017) 248–262.

[50] D.S. Chen, I. Mellman, Oncology meets immunology: the cancer-immunity cycle, Immunity 39 (2013) 1–10.

[51] J. Luo, KRAS mutation in pancreatic cancer, Semin Oncol. 48 (2021) 10–18.

[52] X. Lu, J.W. Horner, E. Paul, X. Shang, P. Troncoso, P. Deng, S. Jiang, Q. Chang, D. J. Spring, P. Sharma, J.A. Zebala, D.Y. Maeda, Y.A. Wang, R.A. DePinho, Effective combinatorial immunotherapy for castration-resistant prostate cancer, Nature 543 (2017) 728–732.

[53] E. Elinav, R. Nowarski, C.A. Thaiss, B. Hu, C. Jin, R.A. Flavell, Inflammation-induced cancer: crosstalk between tumours, immune cells and microorganisms, Nat. Rev. Cancer 13 (2013) 759–771.

[54] N. Nagarsheth, M.S. Wicha, W. Zou, Chemokines in the cancer microenvironment and their relevance in cancer immunotherapy, Nat. Rev. Immunol. 17 (2017) 559–572.

[55] J.M. Romero, B. Grunwald, G.H. Jang, P.P. Bavi, A. Jhaveri, M. Masoomian, S. E. Fischer, A. Zhang, R.E. Denroche, I.M. Lungu, A. De Luca, J.M.S. Bartlett, J. Xu, N. Li, S. Dhaliwal, S.B. Liang, D. Chadwick, F. Vyas, P. Bronsert, R. Khokha, T. L. McGaha, F. Notta, P.S. Ohashi, S.J. Done, G.M. O'Kane, J.M. Wilson, J.J. Knox, A. Connor, Y. Wang, G. Zogopoulos, S. Gallinger, A. Four-Chemokine, Signature Is associated with a T-cell-inflamed phenotype in primary and metastatic pancreatic cancer, Clin. Cancer Res. 26 (2020) 1997–2010.

[56] S. Yu, H. Sha, X. Qin, Y. Chen, X. Li, M. Shi, J. Feng, EGFR E746-A750 deletion in lung cancer represses antitumor immunity through the exosome-mediated inhibition of dendritic cells, Oncogene 39 (2020) 2643–2657.

[57] H. Lv, G. Lv, C. Chen, Q. Zong, G. Jiang, D. Ye, X. Cui, Y. He, W. Xiang, Q. Han, L. Tang, W. Yang, H. Wang, NAD(+) metabolism maintains inducible PD-L1 expression to drive tumor immune evasion, Cell Metab. 33 (2021) 110–127, e115.

[58] C.F. Xu, S. Iqbal, S. Shen, Y.L. Luo, X. Yang, J. Wang, Development of "CLAN" nanomedicine for nucleic acid therapeutics, Small 15 (2019), e1900055.

[59] M. Larsson, W.T. Huang, D.M. Liu, D. Losic, Local co-administration of gene-silencing RNA and drugs in cancer therapy: State-of-the art and therapeutic potential, Cancer Treat. Rev. 55 (2017) 128–135.

[60] A. Marabelle, L. Tselikas, T. de Baere, R. Houot, Intratumoral immunotherapy: using the tumor as the remedy, Ann. Oncol. 28 (2017) xii33–xii43.

[61] I. Melero, E. Castanon, M. Alvarez, S. Champiat, A. Marabelle, Intratumoural administration and tumour tissue targeting of cancer immunotherapies, Nat. Rev. Clin. Oncol. 18 (2021) 558–576.

[62] M.A. Aznar, N. Tinari, A.J. Rullan, A.R. Sanchez-Paulete, M.E. Rodriguez-Ruiz, I. Melero, Intratumoral delivery of immunotherapy-act locally, think globally, J. Immunol. 198 (2017) 31–39.

[63] F. Mansilla, K. Birkenkamp-Demtroder, M. Kruhoffer, F.B. Sorensen, C.L. Andersen, P. Laiho, L.A. Aaltonen, H.W. Verspaget, T.F. Orntoft, Differential expression of DHHC9 in microsatellite stable and instable human colorectal cancer subgroups, Br. J. Cancer 96 (2007) 1896–1903.

[64] Y. Yang, J.M. Hsu, L. Sun, L.C. Chan, C.W. Li, J.L. Hsu, Y. Wei, W. Xia, J. Hou, Y. Qiu, M.C. Hung, Palmitoylation stabilizes PD-L1 to promote breast tumor growth, Cell Res. 29 (2019) 83–86.

[65] S. Spranger, R.M. Spaapen, Y. Zha, J. Williams, Y. Meng, T.T. Ha, T.F. Gajewski, Up-regulation of PD-L1, IDO, and T(regs) in the melanoma tumor microenvironment is driven by CD8(+) T cells, Sci. Transl. Med. 5 (2013) 200ra116.

[66] R.L. Setten, J.J. Rossi, S.P. Han, The current state and future directions of RNAi-based therapeutics, Nat. Rev. Drug Disco 18 (2019) 421–446.

[67] X. Xu, J. Wu, Y. Liu, P.E. Saw, W. Tao, M. Yu, H. Zope, M. Si, A. Victorious, J. Rasmussen, D. Ayyash, O.C. Farokhzad, J. Shi, Multifunctional envelope-type siRNA delivery nanoparticle platform for prostate cancer therapy, ACS Nano 11 (2017) 2618–2627.

[68] H. Mirzaei, F. Yazdi, R. Salehi, H.R. Mirzaei, SiRNA and epigenetic aberrations in ovarian cancer, J. Cancer Res Ther. 12 (2016) 498–508.

[69] B. Hu, L. Zhong, Y. Weng, L. Peng, Y. Huang, Y. Zhao, X.J. Liang, Therapeutic siRNA: state of the art, Signal Transduct. Target Ther. 5 (2020) 101.

[70] F. Wang, T. Zuroske, J.K. Watts, RNA therapeutics on the rise, Nat. Rev. Drug Disco 19 (2020) 441–442.

[71] C. Li, J. Zhou, Y. Wu, Y. Dong, L. Du, T. Yang, Y. Wang, S. Guo, M. Zhang, A. Hussain, H. Xiao, Y. Weng, Y. Huang, X. Wang, Z. Liang, H. Cao, Y. Zhao, X. J. Liang, A. Dong, Y. Huang, Core role of hydrophobic core of polymeric nanomicelle in endosomal escape of siRNA, Nano Lett. 21 (2021) 3680–3689.

[72] W. Sang, Z. Zhang, Y. Dai, X. Chen, Recent advances in nanomaterial-based synergistic combination cancer immunotherapy, Chem. Soc. Rev. 48 (2019) 3771–3810.

[73] A. Rodallec, G. Sicard, R. Fanciullino, S. Benzekry, B. Lacarelle, G. Milano, J. Ciccolini, Turning cold tumors into hot tumors: harnessing the potential of tumor immunity using nanoparticles, Expert Opin Drug Met. 14 (2018) 1139–1147.